Original Article

MOLECULAR METABOLISM

Compound- and fiber type-selective requirement of AMPKγ3 for insulin-independent glucose uptake in skeletal muscle

Philipp Rhein [1,2], Eric M. Desjardins [3,4,14], Ping Rong [5,14], Danial Ahwazi [6], Nicolas Bonhoure [1], Jens Stolte [1], Matthieu D. Santos [7], Ashley J. Ovens [8,9], Amy M. Ehrlich [6], José L. Sanchez Garcia [1], Qian Ouyang [5], Julian M. Yabut [3,4], Mads Kjolby [10,11], Mathieu Membrez [1], Niels Jessen [10,11], Jonathan S. Oakhill [8,9], Jonas T. Treebak [6], Pascal Maire [7], John W. Scott [9,12,13], Matthew J. Sanders [1], Patrick Descombes [1], Shuai Chen [5], Gregory R. Steinberg [3,4], Kei Sakamoto [1,6,*]

ABSTRACT

Objective: The metabolic master-switch AMP-activated protein kinase (AMPK) mediates insulin-independent glucose uptake in muscle and regulates the metabolic activity of brown and beige adipose tissue (BAT). The regulatory AMPKγ3 isoform is uniquely expressed in skeletal muscle and potentially in BAT. Herein, we investigated the role that AMPKγ3 plays in mediating skeletal muscle glucose uptake and whole-body glucose clearance in response to small-molecule activators that act on AMPK via distinct mechanisms. We also assessed whether γ3 plays a role in adipose thermogenesis and browning.

Methods: Global AMPKγ3 knockout (KO) mice were generated. A systematic whole-body, tissue, and molecular phenotyping linked to glucose homeostasis was performed in γ3 KO and wild-type (WT) mice. Glucose uptake in glycolytic and oxidative skeletal muscle *ex vivo* as well as blood glucose clearance in response to small molecule AMPK activators that target the nucleotide-binding domain of the γ subunit (AICAR) and allosteric drug and metabolite (ADaM) site located at the interface of the α and β subunit (991, MK-8722) were assessed. Oxygen consumption, thermography, and molecular phenotyping with a β3-adrenergic receptor agonist (CL-316,243) treatment were performed to assess BAT thermogenesis, characteristics, and function.

Results: Genetic ablation of γ3 did not affect body weight, body composition, physical activity, and parameters associated with glucose homeostasis under chow or high-fat diet. γ3 deficiency had no effect on fiber-type composition, mitochondrial content and components, or insulin-stimulated glucose uptake in skeletal muscle. Glycolytic muscles in γ3 KO mice showed a partial loss of AMPKα2 activity, which was associated with reduced levels of AMPKα2 and β2 subunit isoforms. Notably, γ3 deficiency resulted in a selective loss of AICAR-, but not MK-8722-induced blood glucose-lowering *in vivo* and glucose uptake specifically in glycolytic muscle *ex vivo*. We detected γ3 in BAT and found that it preferentially interacts with α2 and β2. We observed no differences in oxygen consumption, thermogenesis, morphology of BAT and inguinal white adipose tissue (iWAT), or markers of BAT activity between WT and γ3 KO mice.

Conclusions: These results demonstrate that γ3 plays a key role in mediating AICAR- but not ADaM site binding drug-stimulated blood glucose clearance and glucose uptake specifically in glycolytic skeletal muscle. We also showed that γ3 is dispensable for β3-adrenergic receptor agonist-induced thermogenesis and browning of iWAT.

Keywords AMP-activated protein kinase; 5-aminoimidazole-4-carboxamide riboside; MK-8722; TBC1D1; Brown adipose tissue; Beige adipose tissue

[1]Nestlé Research, Société des Produits Nestlé S.A., EPFL Innovation Park, Lausanne, 1015, Switzerland [2]School of Life Sciences, EPFL Innovation Park, Lausanne, 1015, Switzerland [3]Centre for Metabolism, Obesity, and Diabetes Research, McMaster University, Hamilton, ON, L8N3Z5, Canada [4]Department of Medicine and Department of Biochemistry and Biomedical Sciences, McMaster University, Hamilton, ON, L8N3Z5, Canada [5]MOE Key Laboratory of Model Animal for Disease Study, Model Animal Research Center, School of Medicine, Nanjing University, Nanjing, 210061, China [6]Novo Nordisk Foundation Center for Basic Metabolic Research, University of Copenhagen, Copenhagen, 2200, Denmark [7]Université de Paris, Institut Cochin, INSERM, CNRS, 75014, Paris, France [8]Metabolic Signalling Laboratory, St Vincent's Institute of Medical Research, School of Medicine, University of Melbourne, Fitzroy, VIC, 3065, Australia [9]Mary MacKillop Institute for Health Research, Australian Catholic University, Melbourne, VIC, 3000, Australia [10]Department of Biomedicine, Aarhus University, Aarhus, Denmark [11]Department of Clinical Pharmacology and Steno Diabetes Center Aarhus, Aarhus University Hospital, Aarhus, Denmark [12]Protein Chemistry and Metabolism Unit, St Vincent's Institute of Medical Research, Fitzroy, VIC, 3065, Australia [13]The Florey Institute of Neuroscience and Mental Health, Parkville, VIC, 3052, Australia

[14] These authors contributed equally.

*Corresponding author. Novo Nordisk Foundation Center for Basic Metabolic Research, University of Copenhagen, Blegdamsvej 3B, Copenhagen, DK-2200, Denmark. E-mail: kei.sakamoto@sund.ku.dk (K. Sakamoto).

Received March 5, 2021 • Revision received March 21, 2021 • Accepted March 26, 2021 • Available online 30 March 2021

https://doi.org/10.1016/j.molmet.2021.101228

1. INTRODUCTION

AMP-activated protein kinase (AMPK) is an evolutionary conserved energy sensor that functions to maintain energy homeostasis through coordinating metabolic pathways [1,2]. AMPK exists as complexes of three subunits: a catalytic α and two regulatory β and γ subunits. Each exists as multiple isoforms ($\alpha1/\alpha2$, $\beta1/\beta2$, and $\gamma1/\gamma2/\gamma3$), generating up to 12 possible combinations [1]. AMPK heterotrimers are active when a conserved threonine (Thr172) residue within the activation loop of the α subunit kinase domain is phosphorylated [3]. The major upstream kinase phosphorylating Thr172 in metabolic tissues (e.g., muscle, liver) is a complex containing LKB1 [4,5]. The γ-subunits contain four tandem cystathionine β-synthase (CBS) motifs that bind adenine nucleotides. Binding of ADP and/or AMP to the CBS motifs causes conformational changes that promote net Thr172 phosphorylation [6–8]. Moreover, the binding of AMP, but not ADP, further increases AMPK activity by direct allosteric stimulation [6]. Prodrugs of AMP-mimetics such as 5-aminoimidazole-4-carboxamide riboside (AICAR) have been widely used as pharmacological AMPK activators that target the CBS motifs [9]. Proof-of-concept preclinical studies demonstrated that AICAR treatment improved insulin sensitivity in animal models of insulin resistance [10]. However, AICAR produces numerous AMPK-independent metabolic actions [11]. For example, we have recently demonstrated that AICAR suppresses hepatic glucose production independently of AMPK [12] through inhibition of fructose-1,6-bisphosphatase-1, an AMP-sensitive enzyme involved in gluconeogenesis, *in vivo* [13]. We also showed that AICAR regulated >750 genes in AMPK-null primary mouse hepatocytes [14].

A nucleotide-independent mechanism of AMPK regulation was discovered when a novel small-molecule activator, A-769662, was identified [15] and its mechanism of action explored [16–18]. The crystallographic structures of AMPK trimeric complexes revealed that A-769662 and 991 (another activator, also known as ex229) bind in a pocket termed allosteric drug and metabolite (ADaM) site located at the interface of the α subunit (kinase domain N-lobe) and β subunit (carbohydrate binding module) [9,19,20]. A-769662 was subsequently found to be selective for the AMPK$\beta1$-containing complexes [17] and failed to stimulate AMPK-dependent glucose uptake due to lack of potency against $\beta2$-containing complexes that are enriched in skeletal muscle [21]. We and others have shown that 991, and its two related benzimidazole derivatives with improved bioavailability (MK-8722, PF-739), are potent and highly specific AMPK activators [14,22,23]. They activate both $\beta1$- and $\beta2$-containing complexes (thereby activating all 12 possible human AMPK complexes) and have been shown to stimulate glucose uptake in skeletal muscle and lower blood glucose levels *in vivo* [22,24]. Notably, the administration of PF-739 resulted in attenuated blood glucose reduction in skeletal muscle-specific but not in liver-specific double knockout (KO) of AMPK$\alpha1/\alpha2$ [23].

AMPK isoform expression varies among different cell and tissue types, with $\alpha1$, $\beta1$, and $\gamma1$ appearing the most ubiquitously expressed. Conversely, $\gamma3$ is selectively expressed in skeletal muscles containing a high proportion of glycolytic/fast-twitch fibers such as extensor digitorum longus (EDL) muscle [22,25–27]. Interestingly, even though skeletal muscle expresses multiple isoforms, assays of immunoprecipitated isoforms reveal that the $\alpha2\beta2\gamma1$ and $\alpha2\beta2\gamma3$ complexes account for 90% (of which $\alpha2\beta2\gamma3$ accounts for 20%) of the total AMPK trimers in mouse EDL skeletal muscle [21]. Loss of expression/function of $\alpha2$, $\beta2$ or $\gamma3$ is sufficient to ablate AICAR-induced glucose uptake in isolated skeletal muscle *ex vivo* [25,28–32].

In addition to its established metabolic roles in skeletal muscle [33,34], AMPK also plays a vital role in regulating the development of brown adipose tissue (BAT), maintenance of BAT mitochondrial function, and browning of white adipose tissue (WAT) [35]. Adipose-specific AMPK$\beta1/\beta2$-KO (ad-AMPK KO) mice had a profound defect in thermogenesis [36], and both cold exposure and acute treatment with the $\beta3$-adrenergic receptor agonist (CL-316,243) in the ad-AMPK KO mice yielded subnormal increments in oxygen consumption and BAT temperature responses (likely related to impairments in BAT mitochondrial function). A high-throughput screen of protein kinases using a combination of RNAi-mediated knockdown and pharmacological inhibitors identified AMPK as a prominent kinase that promoted the formation of UCP1-abundant brown adipocytes *in vitro* [37]. Proof of concept experiments *in vivo* showed that daily treatment of diabetic ZDF rats with an AMPK activator (C163, for six weeks) increased the formation of brown adipocytes [37]. Intriguingly, transcripts of the *Prkag3* (AMPK$\gamma3$ gene) were identified in brown adipocyte precursors at intermediate levels, and RNAi-mediated knockdown of *Prkag3* was sufficient to profoundly block the brown adipocyte formation without affecting general adipose differentiation [37]. These results prompted us to assess whether $\gamma3$ plays a role in adipose thermogenesis and browning *in vivo*.

We hypothesized that $\gamma3$-containing complexes play an important role for insulin-independent and AMPK activator-mediated glucose uptake in skeletal muscle and for regulating BAT thermogenesis. To test this hypothesis, we generated $\gamma3$ KO mice and determined the effect of AICAR and the ADaM site binding drugs (991, MK-8722) on glucose uptake in glycolytic and oxidative skeletal muscles *ex vivo* and blood glucose kinetics *in vivo*. In addition, we probed BAT function using the $\beta3$-adrenergic receptor agonist CL-316,243. Strikingly, we found that $\gamma3$ deficiency resulted in a selective loss of AICAR-, but not 991/MK-8722-induced blood glucose clearance *in vivo* and glucose uptake specifically in glycolytic muscle *ex vivo*. We also found that $\gamma3$ is not required for the acute $\beta3$-adrenergic receptor-induction of UCP1-mediated non-shivering thermogenesis in the BAT, for the adaptive response to non-shivering thermogenesis or the browning of WAT.

2. MATERIALS AND METHODS

2.1. Materials

5-aminoimidazole-4-carboxamide riboside (AICAR) was purchased from Apollo Scientific (OR1170T; Bredbury, United Kingdom). 991 (5-[[6-chloro-5-(1-methylindol-5-yl)-1H-benzimidazol-2-yl]oxy]-2-methyl-benzoic acid) (CAS#: 129739-36-2) was synthesized by Spirochem (Basel, Switzerland) as previously described [22]. Protein G Sepharose and P81 paper were purchased from GE Healthcare (Chicago, IL, USA). [γ-^{32}P]-ATP was purchased from PerkinElmer (Waltham, MA, USA). The substrate peptide AMARA was synthesized by GL Biochem (Shanghai, China). All other reagents were from MilliporeSigma (Burlington, MA, USA) if not otherwise stated. Lists of primary and secondary antibodies are provided in Supplementary Tables 1 and 2.

2.2. Animal ethics and models

Animal experiments were approved by the internal and local ethics committee and conducted in accordance with the European Convention for the Protection of Vertebrate Animals used for Experimental and Other Scientific Purposes. Protocols used were approved by the Service Vétérinaire Cantonal (Lausanne, Switzerland) under licenses VD3332 and VD3465, and by an ethical committee (Com'Eth, CE17) registered at the French Ministry of Research (Reference #: 10261), and also by the Danish Animal Experiments Inspectorate (Reference #: 2017-15-0202-00058), and were in accordance with McMaster

Animal Care Committee guidelines (AUP #: 16-12-41, Hamilton, ON). Protocols used were also approved by the Ethics Committees at Nanjing University with involved personnel having personal licenses from the regional authority. The generation of a constitutive *Prkag3*$^{-/-}$ (AMPKγ3$^{-/-}$) mice was performed by Taconic Biosciences as described in Supplementary Figure 1. The AMPKα1f/f and AMPKα2f/f mice were generated as previously described [38], and obtained from the Jackson Laboratory (Bar Harbor, ME, USA). These two strains were used to derive AMPKα1f/f/α2f/f mice that were then bred with the Mlc1f-Cre mice to obtain the AMPKα1f/f/α2f/f - Mlc1f-Cre mice. The resultant AMPKα1f/f/α2f/f - Mlc1f-Cre mice were the AMPKα1/α2 skeletal muscle-specific KO mice. All these lines were on C57BL6 background. The animals were kept and maintained according to local regulations under a light–dark cycle of 12 h and had free access to a standard chow diet. Male mice ranging 10–16 weeks of age were used for experiments otherwise stated. High-fat diet (HFD) (60 kcal% fat) was obtained from Research Diet (RD 12492).

2.3. Analysis of body composition and plasma hormone levels

Body composition (fat content, lean tissues and free body fluid) was assessed using the Minispec analyzer (Bruker) by Nuclear Magnetic Resonance (NMR) technology. The test was conducted on conscious fed mice. Blood was collected at the indicated age by retro orbital puncture under isoflurane anesthesia at noon on mice fasted for 4 h. Plasma insulin and leptin levels were measured on a BioPlex analyzer (BioRad) using the Mouse Metabolic Magnetic Hormone Magnetic Bead panel kit (MilliporeSigma).

2.4. Oral glucose tolerance test

Mice were fasted overnight (16 h) and a bolus of glucose solution (2 g/kg body weight) was administered via oral gavage. Blood glucose collected from the tail vein was measured at different time points over 120 min using blood glucose monitor and glucose test strips (Roche Diagnostics, Accu-Chek).

2.5. Preparation of mouse tissue extracts for protein analysis

Mouse tissues were dissected and immediately frozen in liquid nitrogen. The tissues were homogenized in ice-cold lysis buffer (270 mM sucrose, 50 mM Tris·HCl (pH 7.5), 1 mM EDTA, 1 mM EGTA, 1% (v/v) Triton X-100, 20 mM glycerol-2-phosphate, 50 mM NaF, 5 mM $Na_4P_2O_7$, 1 mM DTT, 0.1 mM PMSF, 1 mM benzamidine, 1 μg/mL microcystin-LR, 2 μg/mL leupeptin, and 2 μg/mL pepstatin A) using a tissue lyser (Tissue Lyser II; Qiagen). Lysates were centrifuged at 21,300 *g* for 15 min and protein concentration from the supernatant was determined using Bradford reagent (23200, Thermo Fisher) and bovine serum albumin (BSA) as standard. The supernatants were stored in aliquots in a −80 °C freezer until subsequent analysis.

2.6. Immunoblotting

Protein extracts were denatured in Laemmli buffer at 95 °C for 5 min. Twenty micrograms of protein was separated by SDS-PAGE on 4–12% gradient gels (NW04127, Thermo Fisher) and transferred onto nitrocellulose membranes (#926-31090, LiCOR). Membranes were blocked for 1 h at room temperature in LiCOR blocking buffer (#927-60001, LiCOR). The membranes were subsequently incubated in TBST (10 mM Tris (pH 7.6), 137 mM NaCl, and 0.1% (v/v) Tween-20) containing 5% (w/v) BSA and the primary antibody overnight at 4 °C. After extensive washing, the membranes were incubated for 1 h in either HRP-conjugated or LiCOR secondary antibodies diluted 1:10,000. Signal imaging was performed either using enhanced chemiluminescence (ECL) reagent (GE Healthcare) or a LiCOR Odyssey CLx imaging system. Densitometry for ECL blots was performed using Image J Software (NIH). Because of sample limitation (from the incubated muscle tissue samples), we also utilized automated capillary Western Blot system Sally Sue (ProteinSimple, San Jose, CA, USA). Experiments were performed according to the manufacturer's protocol using the indicated standard reagents for the Sally Sue system (SM-S001, ProteinSimple). Briefly, all samples were first diluted to 2 mg/mL in lysis buffer and then further diluted to 0.5 mg/mL in 0.1% SDS. Following the manufacturer's instructions for sample preparation, this resulted in an assay protein concentration of 0.4 mg/mL.

2.7. Immunoprecipitation and in vitro AMPK activity assay

Lysates of muscle (200 μg) or BAT (1,000 μg) were incubated on a rotating platform at 4 °C overnight with a mix of 5 μL packed protein G-Sepharose and the indicated antibodies. The Sepharose beads were pelleted at 500 *g* for 1 min and initially washed twice with 0.5 mL lysis buffer containing 150 mM NaCl and subsequently washed twice with the same amount of buffer A [50 mM HEPES (pH 7.4), 150 mM NaCl, 1 mM EGTA, and 1 mM DTT]. The immunoprecipitated AMPK complexes were either eluted with Laemmli buffer for immunoblot analysis or used for *in vitro* AMPK activity assay. The AMPK activity assay was performed by incubating the beads (i.e. immune-complexes) for 30 min at 30 °C on a heated shaker in buffer A with additional 10 mM Mg^{2+} and 100 μM ATP in presence of 200 μM AMARA peptide (AMARAASAAALARRR) and 1 μCi of [γ-^{32}P] ATP [22]. Reactions were stopped by spotting the reaction mix onto P81 filter papers and washing in 75 mM phosphoric acid. The P81 papers were dried after three washes and the ^{32}P incorporation into the substrate peptide measured by Cherenkov counting (5 min) using a scintillation counter (Tri-Carb 2810TR, PerkinElmer).

2.8. Citrate synthase activity assay

Protein extracts (10 μg) (using the same lysis buffer described above) was assayed in duplicates using a citrate synthase assay kit (CS0720, MilliporeSigma) according to the manufacturer's instruction using recombinant citrate synthase as positive control.

2.9. Analysis of gene expression and mitochondrial DNA copy number using quantitative real-time PCR (qPCR)

To perform a relative quantification of mRNA levels of the AMPK subunit isoforms in mouse skeletal muscle tissues, reverse transcription and qPCR was performed as described [14]. All the primers and sequences are listed in Supplementary Table 3. Relative mRNA quantities were calculated for triplicate muscle samples from four to five animals and normalized using the three reference genes *Hprt1* (hypoxanthine ribosyltransferase, HPRT), *GusB* (beta-glucuronidase) and *Pgk1* (Phosphoglycerate Kinase 1). Real-time qPCR in BAT was performed separately as described [36]. Relative gene expression was calculated using the comparative Ct ($2-\Delta Ct$) method, where values were normalized to a reference gene (*Ppia*).

To relatively quantify the amount of mtDNA present per nuclear genome by qPCR, mtDNA (16S, ND4) and nuclear DNA (PMP22, Titin) primers and probes were used, the sequences of which are shown in Supplementary Table 3. The relative mt copy number was determined based on the relative abundance of nuclear and mtDNA, calculated as average of the two targets respectively. The relative abundance was then expressed by ΔCT or CT(nDNA) - CT(mtDNA) and displayed as fold change of copy number of mtDNA per nuclear genome compared to the WT muscle.

2.10. Immunofluorescence for fiber type determination and fiber size

For immunostaining against Myh4, Myh2, Myh7 and Laminin, mouse hindlimbs (no skin) without fixation were embedded with Tissue-TEK OCT (Sakura Finetek, Netherlands) and directly frozen in cold isopentane pre-cooled in liquid nitrogen as described [39]. Hindlimb cross sections were prepared using a cryostat (Leica 3050s) with a thickness of 10 μm. The cross sections were washed 3 times for 5 min with PBS and then incubated with blocking solution (PBS and 10% goat serum) for 30 min at room temperature. The sections were incubated overnight with primary antibody diluted in PBS + 10% goat serum solution at 4 °C and washed as described above. The sections were then incubated with secondary antibody, diluted in PBS + 10% goat serum solution for 1 h at room temperature. Sections were further washed and mounted with Mowiol solution and a glass coverslip. Images were collected with a microscope (Olympus BX63F) and a camera (Hamamatsu ORCA-Flash 4.0). Images were analyzed with ImageJ (NIH). Fiber boundaries were defined by the laminin signal and myosin Myh7 (type I), Myh2 (type IIA), and Myh4 (type IIB) heavy chains were quantified. Remaining unlabeled fibers were included for total fiber number and individual proportions of type I, type IIA, and type IIB of that total number calculated. We did not specifically detect and quantify hybrid fibers due to insufficient resolution and lack of established analytical tools.

2.11. Ex vivo skeletal muscle incubation and analysis of glucose uptake

Animals were anesthetized with Avertin [2,2,2-Tribromoehtanol (Sigma-Aldrich #T48402) and 2-Methyl-2-butanol 99% (Sigma-Aldrich #152463)] via an intraperitoneal injection, and EDL or soleus muscles were rapidly dissected and mounted in oxygenated (95% O_2 and 5% CO_2) and warmed (30 °C) Krebs—Ringer buffer in a myograph system (820MS DMT, Denmark). The respective muscles were incubated as described [22,40] in the presence of the indicated drug or vehicle for 50 min. During the last 10 min of the incubation, 2-deoxy-[^{3}H] glucose uptake was measured as described [22,41].

2.12. AICAR and MK-8722 tolerance test

Access of the mice to food was restricted for 3 h (07:00—10:00 h) prior to the experiment. AICAR (250 mg/kg body weight) or vehicle (water) was injected intraperitoneally and blood glucose levels were monitored for 120 min using the Contour XT glucometer (Bayer, Leverkusen) and single use glucose sensors (Ascensia, Basel). MK-8722 tolerance was tested by oral administration of either MK-8722 (10 or 30 mg/kg body weight) or vehicle (0.25% (w/v) methylcellulose, 5% (v/v) Polysorbate 80, and 0.02% (w/v) sodium lauryl sulfate in deionized water) [24]. Blood glucose measurement was performed as described above for the AICAR tolerance test.

2.13. ZMP and adenine nucleotide measurements

Muscle tissues were lysed in 200 μL cold 0.5 M perchloric acid. Extracts were collected and clarified at 14,000 rpm for 3 min. Subsequently, 100 μL clarified lysate was neutralized with 25 μL cold 2.3 M $KHCO_3$ and incubated on ice for 5 min. Samples were centrifuged at 14,000 rpm for 3 min. ZMP were measured by LC-MS/MS with modifications to our previously described method [42]. Both LC and MS instruments were controlled and managed with the Analyst 1.7.1 software (AB Sciex). The autosampler was set at 4 °C and column oven set at 30 °C, which housed a 150 mm (length) × 0.5 mm (inner diameter) Hypercarb 3 μm porous graphitic carbon column (Thermo Fisher Scientific). The LC solvent system comprised 50 mM triethylammonium bicarbonate buffer (TEAB, MilliporeSigma) pH 8.5 in pump A, and acetonitrile with 0.5% trifluoroacetic acid (TFA; MilliporeSigma) in pump B. A flow rate of 400 μl/min was used throughout a gradient program consisting of 0% B (2 min), 0 to 100% B (10 min), 100% B (3 min), 0% B (2 min). Data was analyzed with MultiQuant 3.0.2 software (AB Sciex) using area under the LC curve. Calibration curves were determined by linear regression of the peak area of a ZMP standard curve and were required to have a correlation coefficient (R^2) of >0.98. Adenine nucleotides and adenylate energy charge were measured by LC-MS as described [43].

2.14. Adipose tissue histology

Tissues were fixed in 10% formalin for 24—48 h at 4 °C and processed for paraffin embedding, and hematoxylin and eosin staining by the core histology laboratory at the McMaster Immunology Research Centre (Hamilton, Canada).

2.15. Infrared thermography

UCP1-mediated thermogenesis was assessed in 14-week-old male wild-type (WT) and γ3 KO mice as described [44]. Briefly, mice were anaesthetized with an intraperitoneal injection of 0.5 mg/g body weight Avertin (2,2,2-Tribromoethanol dissolved in 2-methyl-2-butanol; MilliporeSigma) and after 2 min, injected with either saline or the highly selective β3-adrenergic receptor agonist CL 316,243 (Tocris, Bristol, United Kingdom). Mice were subsequently placed dorsal side up onto an enclosed stationary treadmill to measure oxygen consumption (VO_2) with a Comprehensive Laboratory Animal Monitoring System (Columbus Instruments, OH, USA) and 18 min after the second injection a static dorsal thermal image was taken with an infrared camera (FLiR Systems, Wilsonville, OR, USA). Serum samples were collected through tail-nick immediately after the infrared image was taken and non-esterified free fatty acid (NEFA) concentration was determined according to the manufacturer's instructions with a two-step kit (NEFA-HR 2, WAKO).

2.16. Metabolic monitoring

Metabolic monitoring was performed as described [45] in a Comprehensive Laboratory Animal Monitoring System. For the chronic 5-day CL 316,243 challenge, mice were injected intraperitoneally with saline or CL 316,243 (first 4 days 0.5 mg/kg and last day 1.0 mg/kg) at 09:30 h and measurements for VO_2 were calculated 6 h post-injection. Mice were euthanized 24 h after the last injection.

2.17. Statistical analysis

Data are reported as mean ± standard error of the mean (SEM) and statistical analysis was performed using GraphPad Prism software. As indicated in the respective figure legends, differences between only two groups were analyzed using an unpaired two-tailed Student's *t*-test and for multiple comparisons one-way analysis of variance (ANOVA) with Bonferroni *post hoc* test or repeated measures two-way ANOVA was used. Statistical significance was accepted at $P < 0.05$.

3. RESULTS

3.1. A genetic/constitutive loss of the AMPKγ3 reduced AMPKα2 and β2 protein abundance in mouse glycolytic skeletal muscle

We generated constitutive AMPKγ3 KO mice through flanking exons 5—10 of *Prkag3* gene with LoxP sites (Supplementary Figure 1A). This is expected to cause a loss-of-function of the

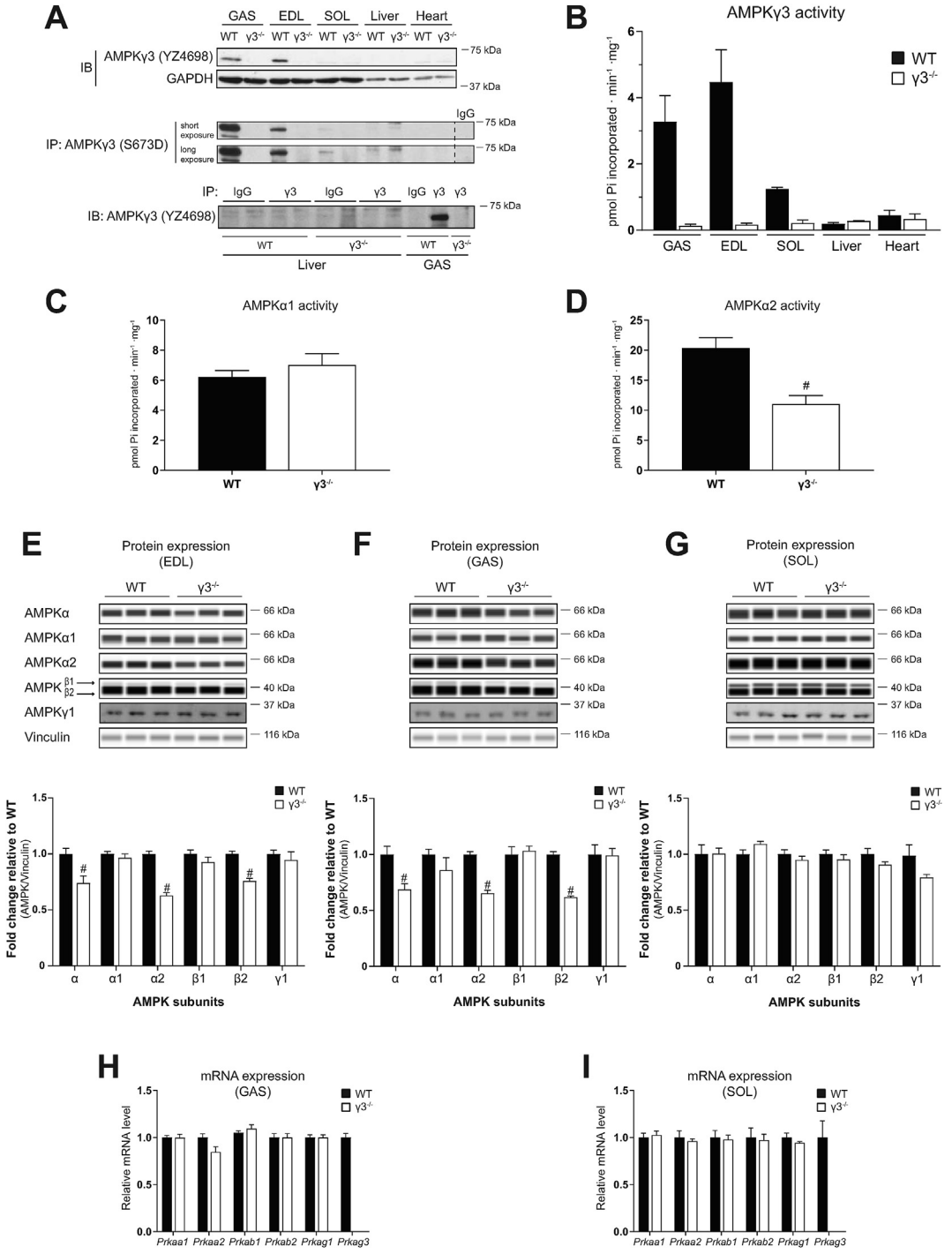

Figure 1: Genetic ablation of the AMPKγ3 causes a significant loss of α2 and β2 expression in mouse glycolytic skeletal muscles. (A) Immunoblot (IB) analysis of γ3 expression in a panel of tissues extracted from wild-type (WT) or AMPKγ3-null ($\gamma3^{-/-}$) mice (upper panel). γ3 expression was further analyzed by immunoblotting following enrichment of the γ3 proteins via immunoprecipitation (IP) from the indicated tissue extracts (200 μg) (middle panel). Liver and skeletal muscle (GAS) tissue extracts from the indicated genotypes were used for immunoprecipitation with either γ3-specific antibody or species-matched IgG (as negative control) and the immune-complexes were subsequently immunoblotted with γ3 antibody (lower panel). (B) The γ3-containing AMPK complexes were immunoprecipitated from the indicated tissues harvested from the indicated genotypes and an *in vitro* AMPK activity assay was performed in duplicate (n = 3 per tissue/genotype). (C, D) The *in vitro* AMPK activity assay was performed on α1- or α2-containing AMPK complexes immunoprecipitated from GAS extracts (n = 9–10 per tissue/genotype). (E–G) Representative immunoblot images and quantification of the AMPK isoform-specific expression using an automated capillary immunoblotting system (Sally Sue) with the indicated antibodies as described in Materials and Methods. AMPK isoform expressions were normalized by their respective vinculin expression (loading control) and are shown as fold change relative to WT. Note that AMPKγ1 expression was quantified using another immunoblotting system (Li-COR, described in the Materials and Methods) due to antibody compatibility (n = 5–11 per tissue/genotype). (H, I) Relative levels of mRNA of the indicated genes (encoding AMPK isoforms) in the indicated skeletal muscles were assessed by qPCR (n = 5 per tissue/genotype). Results are shown as means ± SEM. Statistical significance was determined using the unpaired, two-tailed Student's t-test and are shown as #$P < 0.05$ (WT vs. $\gamma3^{-/-}$). GAS; gastrocnemius, EDL; extensor digitorum longus, SOL; soleus, IgG; immunoglobulin G.

Prkag3 gene by deleting the nucleotide binding cystathionine β-synthase (CBS)-2 domain and parts of the CBS-1 and -3 domains and by generating a frame shift from exon 4 to exon 11 (premature stop codon in exon 12). In addition, the resulting transcript may be a target for non-sense mediated RNA decay and thereby may not be expressed at a significant level. In support of this, we were unable to detect faster migrating polypeptides using the antibody raised against residues 44–64 (within exon 1–3) of the mouse γ3 (Supplementary Figure 1B). γ3 homozygous KO ($\gamma3^{-/-}$) mice were born at expected Mendelian frequency (data not shown). Food intake and spontaneous physical activity, as well as oxygen consumption were similar between WT and γ3 KO mice (Supplementary Figure 1C–E).

We first confirmed a complete loss of γ3 protein and its associated AMPK catalytic activity in tissues harvested from γ3 KO mice (Figure 1A, B). Expression of γ3 is restricted to mouse skeletal muscles containing a high proportion of glycolytic/fast-twitch fibers [22,25]. In line with this, we observed that γ3 and its associated AMPK activity were predominantly detected in glycolytic gastrocnemius (GAS) and extensor digitorum longus (EDL) muscles in WT mice. A modest expression of γ3 and its associated AMPK activity were detected in the soleus muscle (which contains a high proportion of oxidative/slow-twitch fibers) from WT mice when γ3 proteins were enriched by immunoprecipitation prior to the immunoblotting (Figure 1A, B). We detected a faint band immuno-reactive to the γ3 antibody in liver lysates from both WT and γ3 KO mice (Figure 1A, middle panel). We confirmed that the observed band was non-specific as it was readily detected in IgG control samples (Figure 1A, lower panel) and only a negligible background γ3-associated AMPK activity was detected in liver (and also heart) lysates in both WT and γ3 KO mice (Figure 1B). Subsequently, we assessed if loss of γ3 affected AMPKα1- and α2-containing complex activity in GAS muscle. As illustrated in Figure 1C and D, we observed that while AMPKα1 activity was unaltered, AMPKα2 activity was reduced (~50%). Because we and other groups have shown that γ3 predominantly interacts with α2 and β2 [21,22] to form a stable trimeric α2β2γ3 complex, we hypothesized that a constitutive loss of γ3 would cause reduced expressions of α2 and β2 due to their destabilization as monomers. To test this hypothesis, we performed an analysis of AMPK subunit/isoform abundance in both glycolytic (EDL and GAS) and oxidative (soleus) muscles in WT and γ3 KO mice (Figure 1E–G). We previously performed an extensive antibody validation for all AMPKαβγ isoforms using individual isoform-specific KO mouse tissues as negative controls and also reported that γ2 proteins (UniProt ID: Q91WG5 isoform A) were not detectable in mouse skeletal muscles [22]. Immunoblot analysis revealed that protein levels of α2, total AMPKα using a pan α1/α2 antibody, and β2 isoforms were selectively reduced (~20–30%) in EDL and GAS (Figure 1E, F), but not in soleus (Figure 1G), of γ3 KO as compared to WT mice. There was no compensatory increase in γ1 isoform in γ3 KO muscles. To examine whether the reduced protein abundance of α2 and β2 was due to decreased mRNA expression of *Prkaa2* and *Prkab2* (the genes encoding AMPKα2 and β2, respectively) in the γ3 KO mice, we performed qPCR analyses (Figure 1H, I). We confirmed that *Prkag3* mRNA expression was undetectable in skeletal muscle from γ3 KO mice, and observed that there were no differences in mRNA expression of other AMPK subunits/isoforms in GAS (Figure 1H) or soleus (Figure 1I) between WT and γ3 KO mice. Taken together, we have demonstrated that a genetic/constitutive loss of AMPKγ3 causes reduction of AMPKα2 and β2 proteins without affecting their mRNA expressions in glycolytic skeletal muscle.

3.2. AMPKγ3 deficiency has no impact on mitochondrial content and components or fiber-type composition in skeletal muscle

A loss-of-function of skeletal muscle AMPK is associated with reduced mitochondrial content and function [45–48]. Interestingly, a transgenic mouse model overexpressing γ3 mutant (R225Q, a gain-of-function mutation), was associated with higher mitochondrial content and increased amount of a marker of the oxidative capacity (succinate dehydrogenase) in individual muscle fibers of the white portion of GAS [49]. Nevertheless, γ3 deficiency did not cause alterations in mitochondrial content or other parameters in GAS muscle [49]. However, the previously generated γ3 deficient mice did not exhibit significantly reduced expression or activity of AMPKα2 [25], the predominant α-catalytic isoform in skeletal muscle. In the current study, we assessed whether γ3 deficiency, coupled to a partial loss of AMPKα2 activity (Figure 1D), had an impact on mitochondrial parameters in both glycolytic (EDL) and oxidative (soleus) skeletal muscle. We observed no differences in mitochondrial DNA copy number (Figure 2A, B), citrate synthase activity (Figure 2C, D), or components of the mitochondrial respiratory chain complex (Figure 2E, F) in soleus or EDL muscles of WT and γ3 mice. Fiber-type analysis of hindlimb cross sections using immunofluorescence revealed no differences in myosin heavy chain isoform composition in EDL or soleus muscles between the genotypes (Figure 2G, H). We also observed no difference in skeletal muscle fiber size (cross sectional area) between the genotypes (Figure 2I). Collectively, we showed that constitutive γ3 deficiency does not affect mitochondrial content, respiratory chain complex expression, or fiber type composition in both glycolytic and oxidative skeletal muscle.

3.3. AMPKγ3 KO mice exhibit normal glucose homeostasis on chow and in response to high-fat diet (HFD) feeding

Transgenic mice overexpressing the γ3 mutant (R225Q) exhibit an increase in muscle lipid oxidation and are protected against HFD-induced insulin resistance in skeletal muscle [25]. In the current study, we examined whether γ3 deficiency affected glucose homeostasis under standard chow and in response to HFD feeding. Body weight and body composition were similar between WT and γ3 KO mice during both chow and HFD-feeding periods (Figure 3A, B). We observed similar levels of plasma insulin and leptin on chow diet between WT and γ3 KO mice, with their levels increased in a comparable manner for both genotypes in response to HFD feeding (Figure 3C, D). Consistent with these results, we observed comparable fasted blood glucose levels and no difference in glucose tolerance between the genotypes irrespective of the diets (Figure 3E). To complement these *in vivo* results, we assessed insulin signaling and glucose uptake in isolated EDL muscle *ex vivo*. As shown in Figure 3F, basal glucose uptake and Akt phosphorylation were comparable between WT and γ3 KO mice and insulin equally stimulated both parameters in both genotypes. We also confirmed that there was no difference in the expression of GLUT4 and hexokinase II in EDL muscle between WT and γ3 KO mice (Figure 3F). Taken together, these results suggest that γ3 is dispensable for maintenance of glucose homeostasis on chow and in response to HFD.

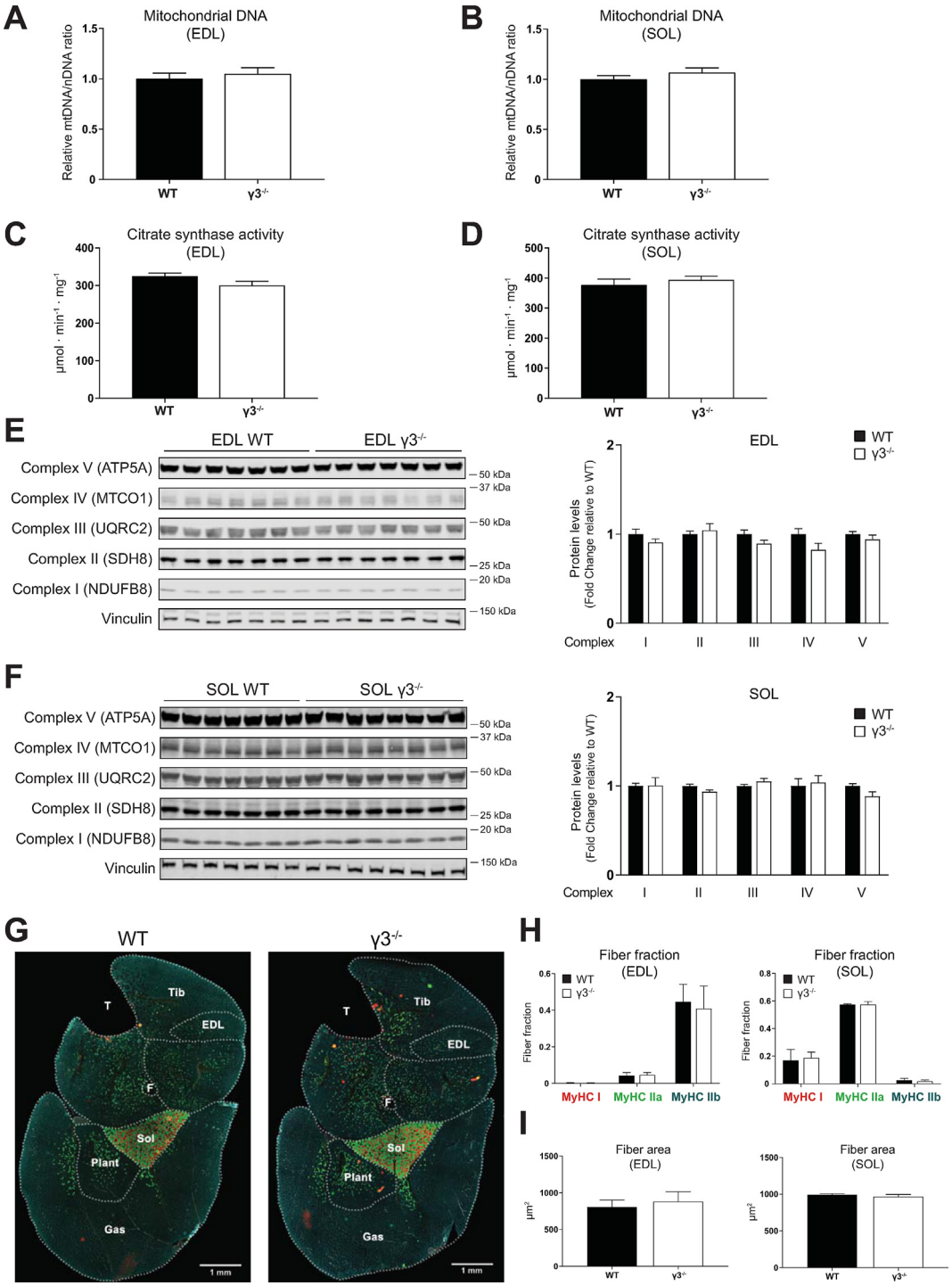

Figure 2: AMPKγ3 deficiency does not affect mitochondrial content and components, or fiber-type composition in skeletal muscles. (A, B) Relative quantification of mitochondrial DNA (mtDNA) was performed using qPCR-based assay as described in the Materials and Methods (n = 5 per tissue/genotype). (C, D) Citrate synthase activity was measured in the indicated muscle extracts (n = 8 per tissue/genotype). (E, F) Immunoblot analysis and quantification of mitochondrial complexes in the indicated muscles (n = 7 per tissue/genotype). (G–I) Representative cross-sectional images (n = 4 per genotype) of the whole-hindlimb muscle fiber-type analysis of the indicated genotypes using isoform-specific myosin heavy chain (MyHC) and laminin antibodies followed by immunofluorescent signal detection (G). Scale bar = 1 mm. Quantification of relative isoform-specific MyHC composition/fraction (red: MyHC I, green: MyHC IIa, blue: MyHC IIb, laminin: gray/white) and fiber area in the indicated muscles were performed as described in Materials and Methods. Unstained fibers are not included in the fiber fraction analysis (H, L, n = 3–4 per tissue/genotype). Results are shown as means ± SEM. GAS; gastrocnemius, EDL; extensor digitorum longus; SOL; soleus, Tib; tibialis anterior, Plant; plantaris, F; fibula, T; tibia.

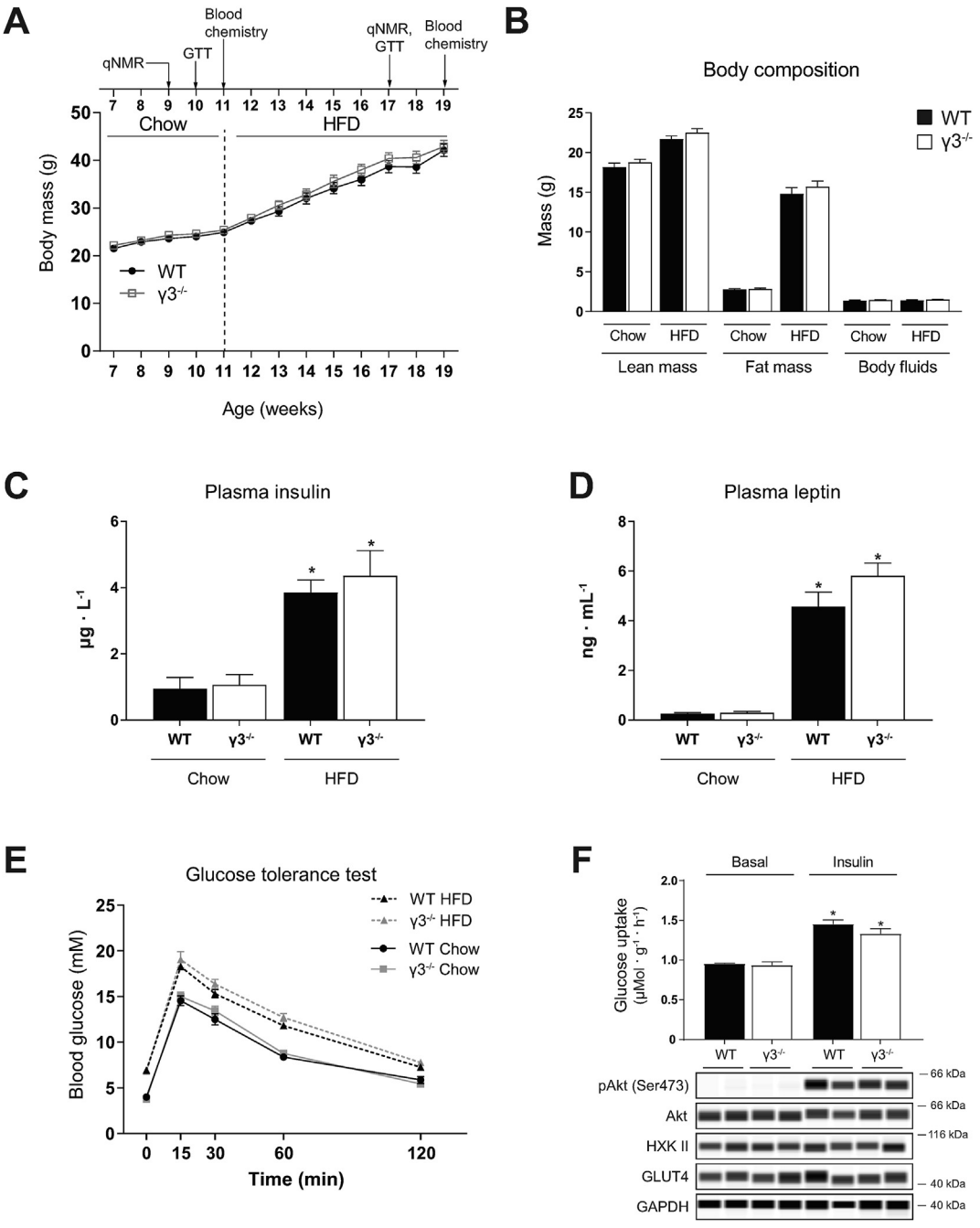

Figure 3: AMPKγ3 is dispensable for maintaining glucose homeostasis under chow and high-fat diet (HFD) feeding. (A) Time sequence of the diet intervention, analysis of body composition (qNMR), oral glucose tolerance test (GTT) and plasma hormone analysis (blood chemistry). Mice were fed chow diet after weaning until 11 weeks of age before switching to HFD (60 kcal% fat). Body weight over time of the indicated genotypes (n = 10 per genotype). (B) Body composition determined by qNMR in the indicated genotypes during the indicated diet treatment. (C, D) Plasma insulin and leptin levels were determined using the commercial enzyme-linked immunosorbent assay kits. (E) Mice were fasted overnight and an oral GTT test was performed during chow (week 10) and HFD (week 17) feeding by monitoring blood glucose kinetics over the indicated duration following an oral administration of a bolus of glucose solution (2 g/kg body weight). (F) Extensor digitorum longus (EDL) muscles from the indicated genotypes on chow diet (10- to 12-week old males from a separate cohort, n = 5–7 per genotype) were isolated in incubated in the presence or absence of insulin (100 nM) for 50 min and were subjected to glucose uptake assay and immunoblot analysis using the indicated antibodies. Results are shown as means ± SEM. Statistical significance was determined using the unpaired/two-tailed Student's t-test or one-way analysis of variance with Bonferroni correction and are shown as $*P < 0.05$ (treatment effect within the same genotype).

3.4. AMPKγ3 deficiency causes attenuated AICAR-stimulated glucose uptake in glycolytic skeletal muscle ex vivo and blood glucose lowering in vivo

AICAR-stimulated glucose uptake in skeletal muscle requires functional AMPK [34]. Consistent with previous studies [30,41], AICAR promoted glucose uptake robustly in EDL (~2.5-fold) and modestly in soleus (~1.6-fold) *ex vivo* in WT mice (Figure 4A, B). Interestingly, we observed that AICAR-stimulated glucose uptake was profoundly reduced in EDL, but not in soleus, in γ3 KO mice (Figure 4A, B). To examine whether a loss of γ3 affected AICAR-induced AMPK activity,

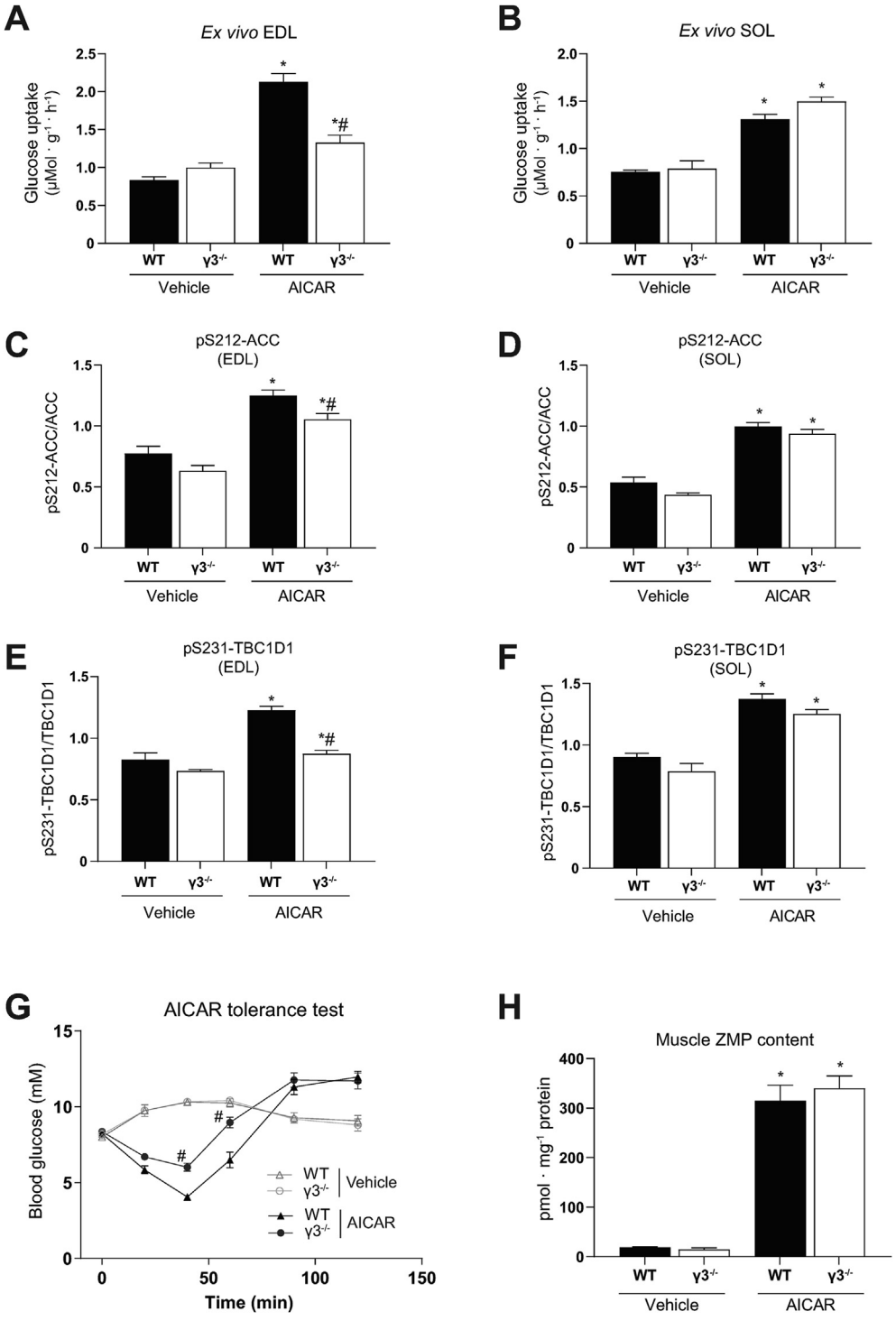

Figure 4: AMPKγ3 is required for AICAR-induced glucose uptake in glycolytic skeletal muscles and hypoglycemia. (A–F) EDL or SOL muscles were isolated from the indicated genotypes and incubated in the absence (vehicle, 0.1% DMSO) or presence of AICAR (2 mM) for 50 min followed by an additional 10-min incubation with the radioactive 2-deoxy-glucose tracer. One portion of the muscle extracts was subjected to glucose uptake measurement (A, B) and the other was used for immunoblot analysis using the automated capillary immunoblotting system with the indicated antibodies (C–F) ($n = 4–7$ per treatment/genotype). (G, H) AICAR tolerance test and muscle ZMP analysis. Mice were fasted for 3 h and injected either with vehicle (water) or AICAR (250 mg/kg body weight, i.p.) followed by blood glucose kinetics measurement over the indicated duration (G). Following the AICAR tolerance test, mice were euthanized and GAS muscles were extracted and ZMP levels were determined (H) ($n = 5–12$ per treatment/genotype). Results are shown as means ± SEM. Statistical significance was determined using the unpaired/two-tailed Student's t-test or one-way analysis of variance (ANOVA) with Bonferroni correction or two-way ANOVA and are shown as $*P < 0.05$ (treatment effect within the same genotype), $\#P < 0.05$ (WT vs. $\gamma3^{-/-}$ within the same treatment). GAS; gastrocnemius, EDL; extensor digitorum longus, SOL; soleus, AICAR; 5-aminoimidazole-4-carboxamide ribonucleoside, ZMP; AICAR monophosphate.

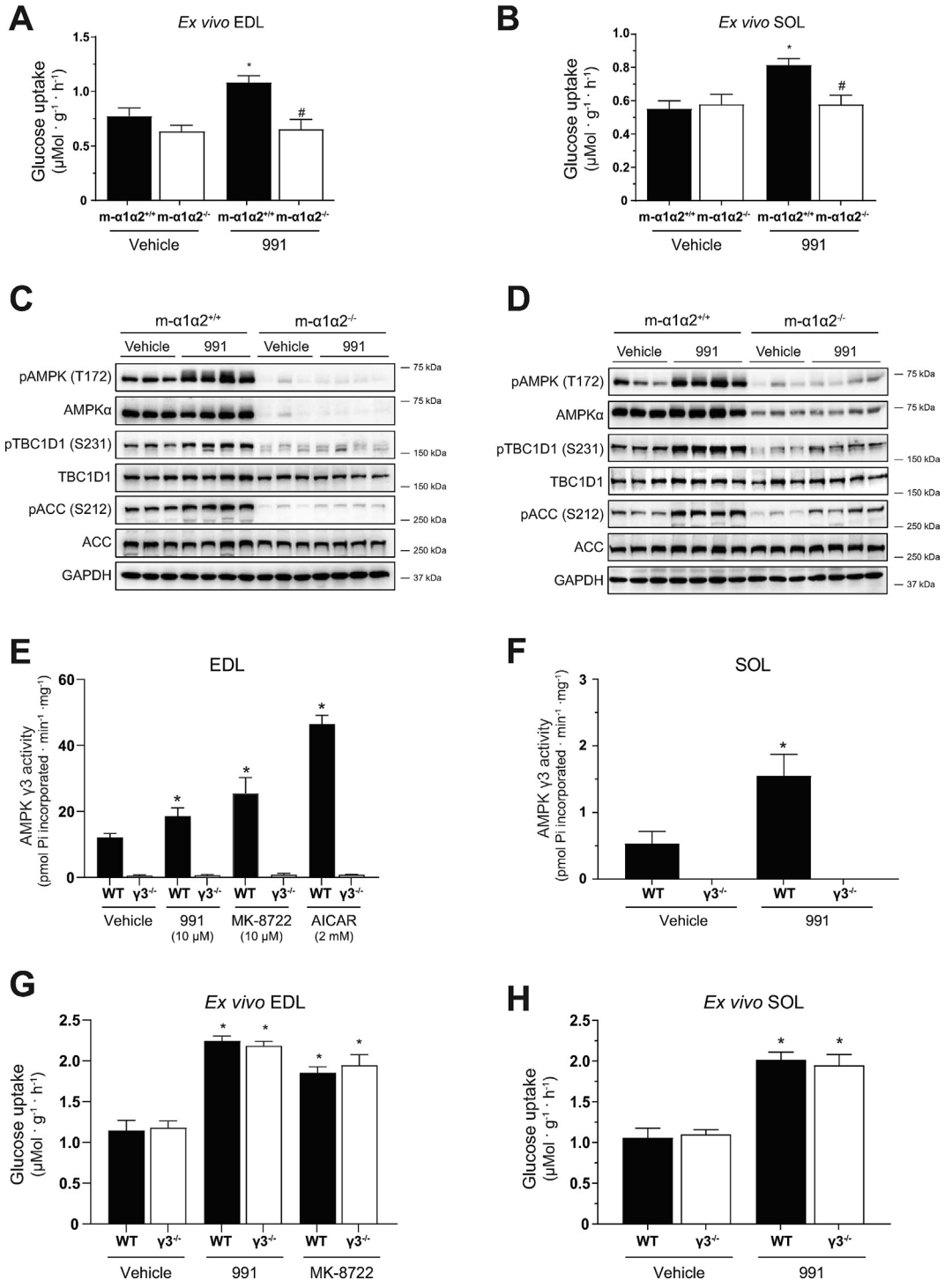

Figure 5: AMPKα1/α2, but not γ3, is required for glucose uptake skeletal muscles and hypoglycemia in response to the ADaM site-targeted activators, 991 and MK-8722. (A—D) EDL or SOL muscles were isolated from the indicated genotypes and incubated in the absence (vehicle, 0.1% DMSO) or presence of 991 (10 μM) for 50 min followed by an additional 10-min incubation with the radioactive 2-deoxy-glucose tracer. One portion of the muscle extracts was subjected to glucose uptake measurement (A, B) and the other was used for immunoblot analysis using the indicated antibodies (followed by a signal detection using enhanced chemiluminescence) (C, D, n = 3—4 per treatment/genotype). (E—L) EDL or SOL muscles were isolated from the indicated genotypes and incubated in the absence (vehicle, 0.1% DMSO) or presence of the indicated compounds for 50 min followed by an additional 10-min incubation with the radioactive 2-deoxy-glucose tracer. One portion of the muscle extracts was subjected to immunoprecipitation with the γ3 antibody followed by an *in vitro* AMPK activity assay (E, F, n = 4—14). The other portion was subjected to glucose uptake measurement (G, H, n = 4—9) or immunoblot analysis using the automated capillary immunoblotting system with the indicated antibodies (I—L, n = 4—9). (M) MK-8722 tolerance test. Mice were fasted for 3 h and orally treated either with vehicle or MK-8722 (10 mg/kg body weight) followed by blood glucose kinetics monitoring over the indicated duration. Results are shown as means ± SEM. Statistical significance was determined using the unpaired/two-tailed Student's t-test or one-way analysis of variance (ANOVA) with Bonferroni correction or two-way ANOVA and are shown as $*P < 0.05$ (treatment effect within the same genotype), $\#P < 0.05$ (WT vs. $\gamma3^{-/-}$ within the same treatment). EDL; extensor digitorum longus; SOL; soleus, AICAR; 5-aminoimidazole-4-carboxamide ribonucleoside.

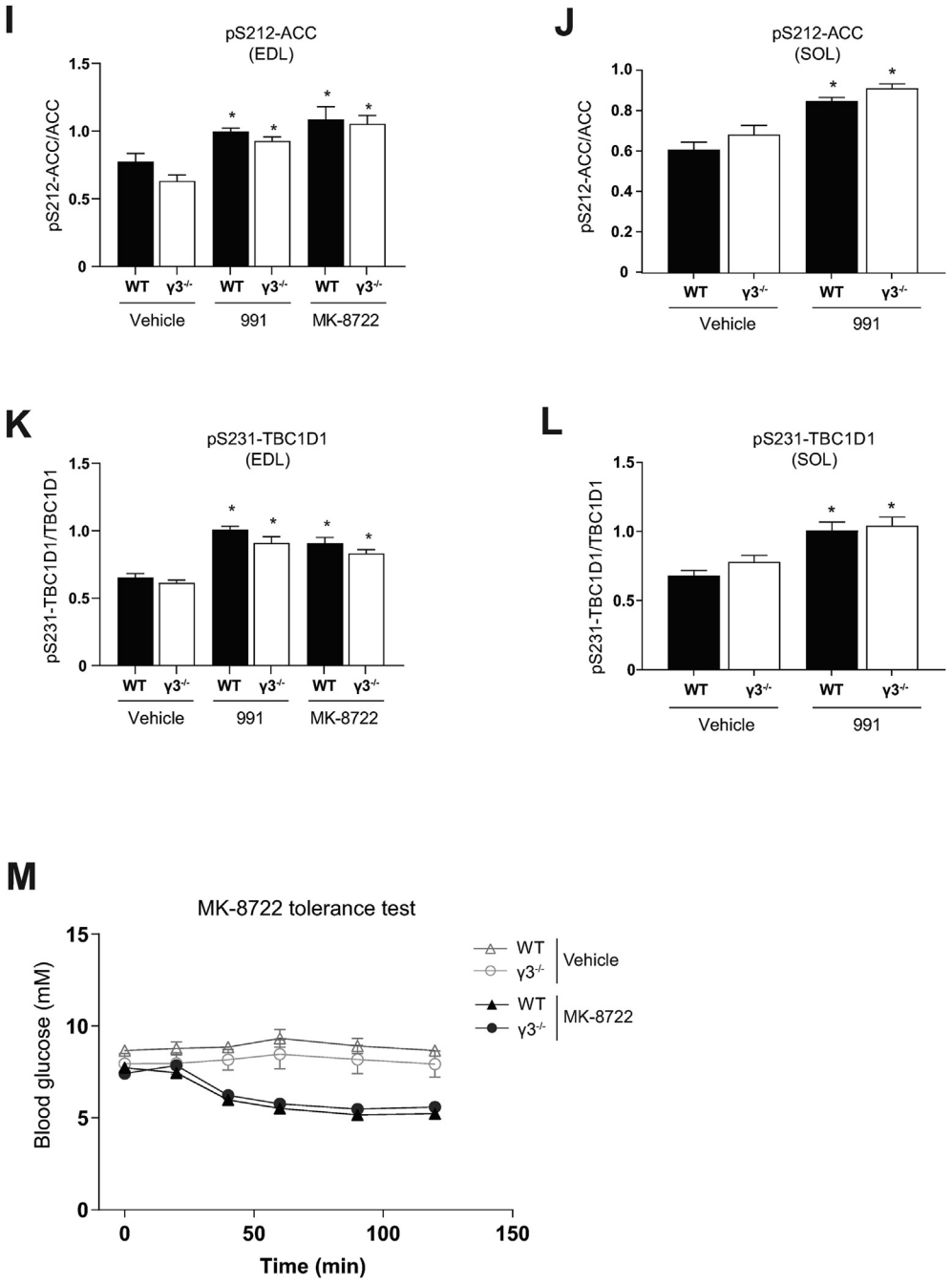

Figure 5: (*continued*).

we measured the phosphorylation of ACC and TBC1D1, established surrogate markers of cellular AMPK activity in muscle. As shown in Figure 4C—F, the phosphorylation of ACC and TBC1D1 was increased in both EDL and soleus in response to AICAR in WT mice. The AICAR-mediated increase in the phosphorylation of ACC and TBC1D1 was reduced in EDL, but not in soleus, in γ3 KO mice (Figure 4C—F). We confirmed that there is no sex-dependent AICAR effect, as AICAR-stimulated glucose uptake was similarly reduced in EDL muscle from female γ3 KO mice (data not shown). We investigated whether a partial loss of γ3 results in a reduction of AICAR-stimulated glucose uptake in EDL. Heterozygous $\gamma3^{+/-}$ mice had ∼50% reduction in γ3 expression in GAS, but the expression of total AMPKα, α2 and β1/β2 was not reduced (Supplementary Figure 2A and B). Incubation of EDL with AICAR *ex vivo* resulted in similar increases in γ3-associated activity and glucose uptake, as well as phosphorylation of ACC and TBC1D1 in both WT and heterozygous $\gamma3^{+/-}$ mice (Supplementary Figure 2C—G).

We subsequently wanted to determine whether γ3 deficiency affected the hypoglycemic effects of AICAR *in vivo*. We utilized briefly fasted animals (3 h fast, 07:00—10:00), as the AICAR-induced reduction of blood glucose in overnight fasted (16 h) mice is predominantly caused by the suppression of hepatic glucose output [13]. After administration

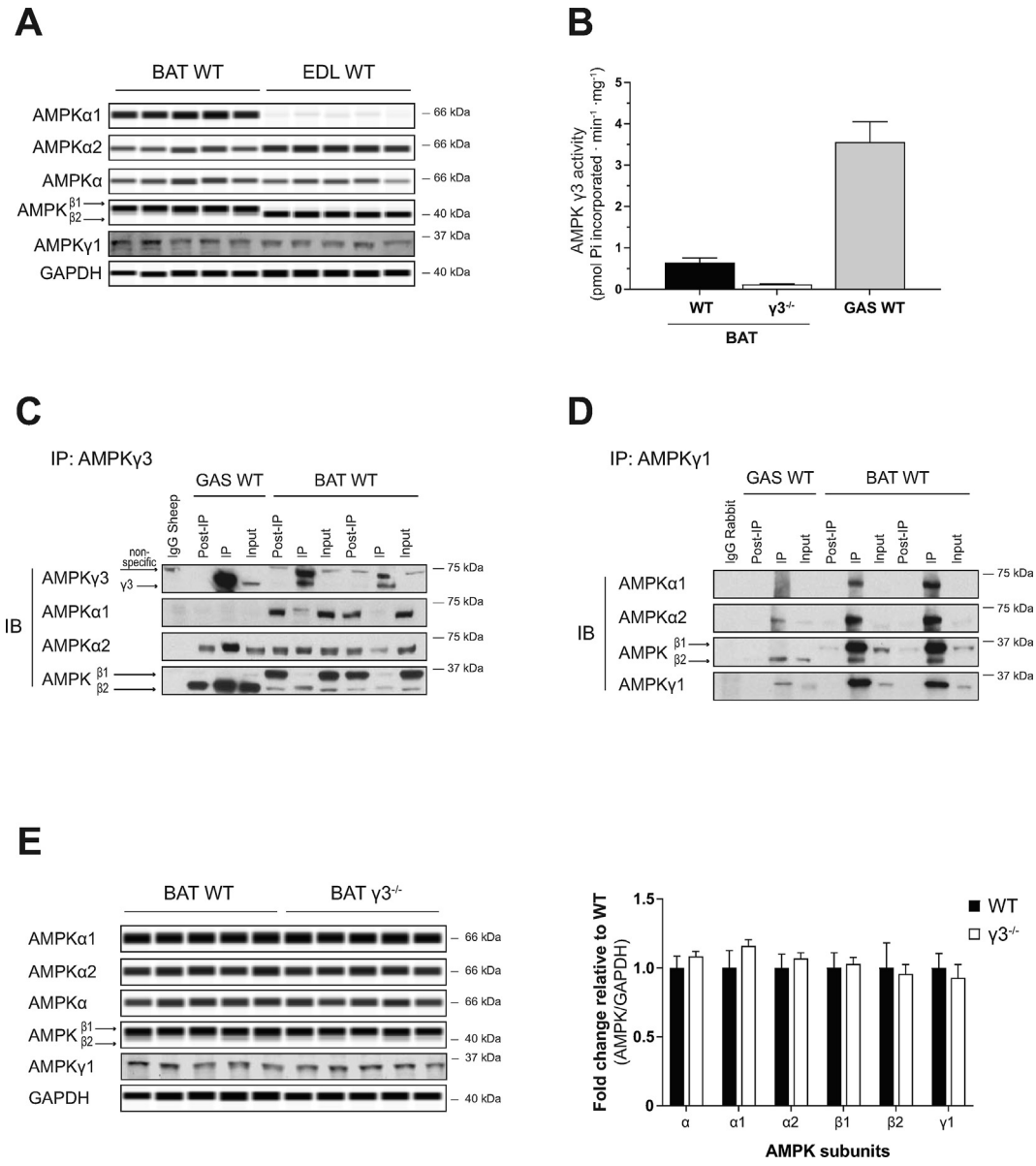

Figure 6: AMPKγ3 is expressed and forms functional trimeric complexes in mouse brown adipose tissue (BAT). (A) Immunoblot (IB) analysis of the skeletal muscle (EDL) and BAT extracts harvested from wild-type (WT) mice using the automated capillary immunoblotting system with the indicated antibodies. Note that γ1 expression was quantified using another immunoblotting system (Li-COR) due to antibody compatibility. (B) Extracts from GAS muscle (100 μg) or BAT (1,000 μg) were subjected to immunoprecipitation (IP) with γ3 antibody and the γ3-containing immune-complexes were assayed for AMPK activity *in vitro*. (C, D) γ3- or γ1-containing AMPK complexes were immunoprecipitated from GAS (100 μg) or BAT (1,000 μg) extracts and subsequently subjected to immunoblot analysis using the indicated antibodies followed by a signal detection using enhanced chemiluminescence. (E) Quantification of the isoform-specific AMPK expression of a panel of tissues (harvested from WT or $\gamma3^{-/-}$ mice) was performed using the automated capillary immunoblotting system with the indicated antibodies. Results are shown as means ± SEM (n = 5–7). GAS; gastrocnemius, EDL; extensor digitorum longus.

of a bolus of AICAR (250 mg/kg body weight, i.p.) or vehicle, we monitored blood glucose kinetics for 2 h in WT and γ3 KO mice. As shown in Figure 4G, we observed that the blood glucose-lowering action of AICAR was blunted (40 and 60 min time points) in γ3 KO compared to that in WT mice. We confirmed that ZMP content in GAS muscle following AICAR administration was comparably increased between the two genotypes (Figure 4H). Additionally, AICAR did not affect adenylate energy charge in GAS from both genotypes (Supplementary Figure 2H). Collectively, these results suggest that γ3 (i.e. γ3-containing AMPK complex(es)) plays an important role in AICAR-mediated glucose uptake and disposal in glycolytic skeletal muscles.

3.5. ADaM site-targeted activators normally stimulate glucose uptake in skeletal muscle and lower blood glucose levels in AMPKγ3 KO mice

The ADaM site-binding pan AMPK activator, 991, robustly stimulates glucose uptake in isolated mouse skeletal muscle tissues *ex vivo* [22,50]. We initially confirmed that the 991-stimulated glucose uptake was fully dependent on AMPK in both EDL and soleus using skeletal

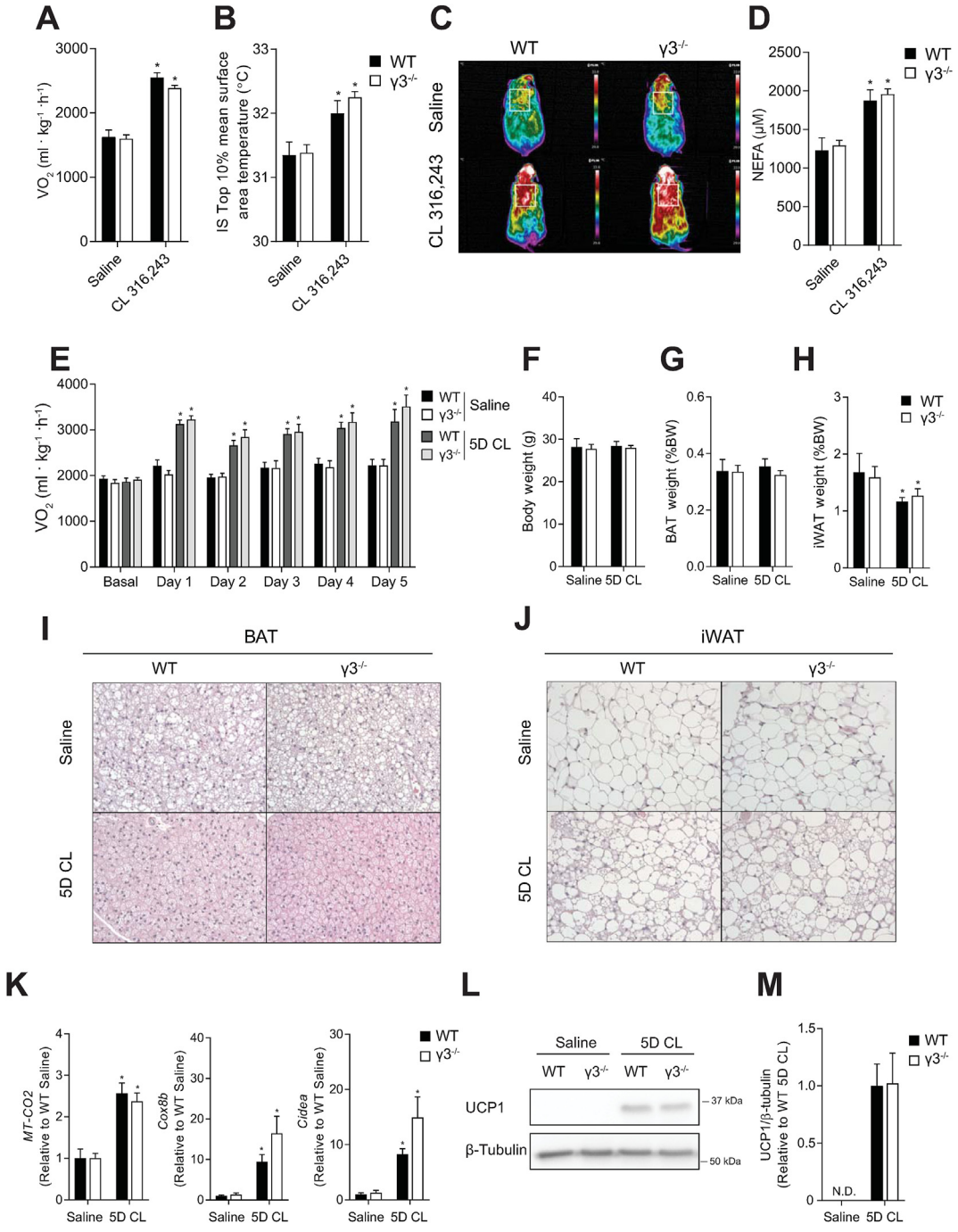

Figure 7: AMPK γ3 is not required for the acute activation of non-shivering thermogenesis or the browning of inguinal white adipose tissue (WAT) in mice. (A) Oxygen consumption (VO_2), (B, C) Interscapular brown adipose tissue (BAT) surface area temperature with representative thermal images, and (D) serum non-esterified free fatty acid (NEFA) concentration in response to a single injection of saline or CL 316,243 in male WT or $\gamma3^{-/-}$ mice (0.033 nmol/g, 20 min time-point), n = 9–13 per group. Data are means ± SEM with a CL 316,243 effect shown as $^{*}P < 0.05$, as determined via repeated measures two-way ANOVA. (E) Oxygen consumption (VO_2) basally and 6-h post-injection of saline or CL 316,243 in male WT or $\gamma3^{-/-}$ mice on indicated days, n = 5–8 per group. (F) Final body weight (BW), (G) BAT weight, and (H) inguinal WAT (iWAT) depot weight following 5 consecutive days of saline or CL 316,243 (5D CL) injections in male WT or $\gamma3^{-/-}$ mice, n = 5–8 per group. (I, J) Representative histological images of H&E-stained BAT (I) and iWAT (J) (10× magnification) from male WT or $\gamma3^{-/-}$ mice treated with saline or 5D CL. K) mRNA expression of genes indicative of iWAT browning, *MT-CO2* (n = 4–8 per group), *Cox8b* (n = 5–8 per group), and *Cidea* (n = 5–7 per group) in male WT or $\gamma3^{-/-}$ mice treated with saline or 5D CL for 5 days. L) Immunoblot analysis and densitometry quantification (M) of UCP1 in male WT and $\gamma3^{-/-}$ mice treated with saline or 5D CL for 5 days (n = 6–8 per group). Data are means ± SEM with $^{*}P < 0.05$ denoting a 5D CL effect, as determined by repeated measures two-way ANOVA (A) and regular two-way ANOVA. N.D.; not detectable

muscle-specific AMPKα1/α2 double KO (m-α1/α2 DKO) mice (Figure 5A, B). Immunoblot analysis validated AMPKα deficiency and profound decreases in the phosphorylation of ACC and TBC1D1 in the absence or presence of 991 in both EDL and soleus in the m-α1/α2 DKO mice (Figure 5C, D). We subsequently assessed the effect of 991, MK-8722 (a structural analog of 991 [24]), and AICAR on γ3-associated AMPK activity in isolated muscle from WT and γ3 KO *ex vivo*. As shown in Figure 5E, γ3-associated activity was increased (∼1.5–2-fold) with 991 or MK-8722 and robustly increased (∼3-fold) with AICAR in EDL from WT mice. Despite minimal γ3-associated activity detectable in soleus, the activity was increased ∼3-fold with 991 in WT mice (Figure 5F). As expected, there was no γ3-associated AMPK activity present in skeletal muscle from γ3 KO mice (Figure 5E, F). In contrast to the effect of AICAR, incubation of EDL with 991 or MK-8722 resulted in comparable increases in glucose uptake in WT and γ3 KO mice (Figure 5G). We also observed that 991-stimulated glucose uptake was similar in soleus between WT and γ3 KO mice (Figure 5H). We noted that 991 and/or MK-8722 increased phosphorylation of ACC and TBC1D1 in EDL and soleus with no differences in the levels of phosphorylation between WT and γ3 KO mice (Figure 5I–L). Consistent with the *ex vivo* results, oral administration of MK-8722 (10 or 30 mg/kg body weight) resulted in a comparable blood glucose-lowering kinetics *in vivo* between WT and γ3 KO mice (Figure 5M and Supplementary Fig. 3). Taken together, we demonstrated that γ3 is dispensable for the stimulation of glucose uptake and disposal in skeletal muscle in response to 991 or MK-8722 (ADaM site targeted compounds).

3.6. AMPKγ3 protein and its associated AMPK trimeric complexes are present in mouse BAT

Prkag3 mRNA are expressed in mouse brown adipose precursors [37]; however, whether γ3 proteins are expressed and exist as part of functional AMPK trimeric complexes in BAT is unknown. We initially performed a comparison of AMPK subunit/isoform protein expression profiles between skeletal muscle (EDL) and BAT from WT mice, which revealed distinct profiles between the two tissues (Figure 6A). Compared to skeletal muscle, BAT expresses relatively higher and lower amounts of α1 and α2, respectively. The total AMPKα content (assessed by a pan-AMPKα antibody) was similar between the tissues. However, the efficacy of the isoform-specific detection of α1 and α2 proteins by this antibody is unknown. We observed a divergent expression pattern of the β isoforms between the tissues. While skeletal muscle predominantly expresses β2, BAT predominantly expresses β1 (Fig. 6A). Conversely, γ1 expression is similar between the tissues. We subsequently immunoprecipitated γ3 from BAT (and GAS muscle as control) and performed either γ3-associated AMPK activity assay or immunoblot analysis to identify α and β subunit isoforms interacting with γ3. As shown in Figure 6B, we detected γ3 and its associated AMPK activity in BAT from WT, but not from γ3 KO mice. Interestingly, γ3 preferentially interacts with α2 and β2 (Fig. 6C), whereas γ1 interacts with α1/α2 and preferentially with β1 (Fig. 6D). We also observed that γ3 deficiency in BAT did not affect the abundance of other AMPK subunit isoforms (Fig. 6E). Collectively, we provide evidence that AMPKγ3 protein is expressed in BAT and it forms functional complexes by mainly interacting with α2 and β2.

3.7. AMPKγ3 is not required for the acute induction of UCP1-mediated non-shivering thermogenesis in the BAT

AMPK plays an important role for BAT formation [37] and thermogenesis in response to cold exposure and β3-adrenoreceptor (β3-AR) stimulation in rodents [36]. We probed BAT function using the β3-AR agonist CL-316,243 (CL), which increases thermogenesis through a UCP1-dependent mechanism [44]. A single injection of CL increased oxygen consumption and interscapular BAT surface area temperature in both WT and γ3 KO mice; however, there were no differences between the genotypes (Figure 7A–C). Furthermore, CL increased serum non-esterified free fatty acid concentration to a similar extent in both WT and γ3 KO mice, indicating no major alterations in lipolysis (Fig. 7D).

3.8. AMPKγ3 is not required for the adaptive response to non-shivering thermogenesis or the browning of inguinal white adipose tissue (iWAT)

We subsequently performed injections of CL for five consecutive days to determine whether γ3 is required for the adaptive response to non-shivering thermogenesis or the browning of iWAT. Daily treatment of mice with CL increased oxygen consumption without altering body or BAT weight, but did reduce iWAT weight similarly in both WT and γ3 KO mice (Figure 7E–H). Furthermore, γ3 KO mice treated with CL for five days had similar morphological changes in BAT — with smaller lipid droplets — and the appearance of multilocular adipocytes within iWAT (Figure 7I, J). Finally, CL treatment increased UCP1 expression (at both transcript and protein levels), as well as levels of other thermogenic and mitochondrial genes such as *Cox2*, *Cox8b*, *and Cidea* in both WT and γ3 KO mice (Fig. 7K–M). These results demonstrate that γ3 is dispensable for β-adrenergic-induced remodeling of BAT and iWAT in mice.

4. DISCUSSION

AMPK has been considered as a promising target for the treatment of metabolic syndrome over the last few decades. The identification of new mechanisms for drug targeting on AMPK (i.e. discovery of the ADaM site) has advanced the development of more potent and selective AMPK activators with improved bioavailability [9]. Recent proof-of-concept studies in rodents and non-human primates have compellingly demonstrated that oral administration of pan AMPK activators (e.g. MK-8722, PF-739) targeting the ADaM site can promote glucose uptake in skeletal muscle, and ameliorate insulin resistance and reduce hyperglycemia without causing hypoglycemia [23,24]. Since γ3 is exclusively expressed in skeletal muscle, understanding of the physiological roles that γ3 plays in regulating glucose metabolism/homeostasis is important for the development of skeletal muscle-selective AMPK activators. In addition, a recent *in vitro* study that reported that γ3 plays a role in BAT development [37] prompted us to investigate the role for γ3 in thermogenesis and adipose browning *in vivo*. In the current study, we found that genetic ablation of γ3 resulted in a selective loss of AICAR-, but not MK-8722-induced blood glucose-lowering *in vivo* and glucose uptake specifically in glycolytic muscles *ex vivo*. We also found that γ3 is dispensable for the acute induction of UCP1-mediated non-shivering thermogenesis in BAT or the adaptive response to non-shivering thermogenesis and the browning of WAT.

We observed that the levels of α2 and β2 isoforms were reduced (∼20–30%) in glycolytic (GAS and EDL), but not in oxidative (soleus) muscle in $\gamma3^{-/-}$ KO compared to WT mice. In soleus, a previous study reported that γ3 was only detectable in a complex with α2 and β2, but relative amount of this complex was shown to be only 2% and >90% of α2 and β2 forms complexes with γ1 [21,34]. Conversely, α2 and β2 form complexes with γ1 (70%) and γ3 (20%), respectively in EDL muscle. Therefore, it is plausible that a constitutive deficiency of γ3 resulted in a partial loss of α2 and β2 proteins due to degradation of

excess monomeric forms of α2 and β2 in GAS/EDL, but not in soleus muscle. Consistent with this notion, a constitutive deletion of γ1, a ubiquitously expressed γ isoform across tissues, resulted in much more profound reductions of all its interacting AMPK isoforms (α1, α2, β1, and β2) in mouse tissues including skeletal muscle [51]. Even though previous work reported that γ3 deficiency did not affect the levels of other AMPK isoforms in GAS muscles, there was a ∼25% reduction of α2 protein expression in GAS muscles from γ3 KO compared to WT mice [25]. It might be the case that it did not reach statistical significance due to insufficient power. In line with this assumption, phosphorylation of AMPKα (Thr172) was reduced in EDL from the same γ3 KO mouse model (compared to WT) [52].

A complete loss of functional α2 or β2 was associated with ablated glucose uptake with AICAR in mouse skeletal muscle *ex vivo* [28,30,31]. To our knowledge, whether a partial loss of α2 and/or β2 (e.g. in heterozygous $\alpha2^{+/-}$ or $\beta2^{+/-}$ mice) reduces glucose uptake in EDL with AICAR *ex vivo* is unknown. However, we previously demonstrated that a profound reduction (>60%) of α2 activity observed in EDL of the LKB1 hypomorphic mice resulted in comparable AICAR-stimulated glucose uptake and ACC phosphorylation compared to WT mice [4]. Moreover, we herein report that 991/MK-8722 stimulates glucose uptake in EDL muscle from the γ3 KO mice. Therefore, a partial reduction of α2/β2 expression (∼20−30%) is unlikely to be responsible for the decrease in AICAR-stimulated glucose uptake in γ3-deficient EDL muscle.

One of the major findings of the present study was that γ3-deficiency caused blunted glucose uptake in EDL *ex vivo* and hypoglycemic response *in vivo* with AICAR, but not with ADaM site-targeted compounds (i.e. 991, MK-8722). This was particularly intriguing as both AICAR and 991/MK-8722 require intact AMPK catalytic activity to promote glucose uptake in skeletal muscle tissues/cells [23,24,28–32,45,50], and we report here that both AICAR and 991/MK-8722 increased γ3-associated AMPK activity. The dose of AICAR (2 mM) used had a more potent effects on γ3-associated activity (∼3-fold increase) as compared to 10 μM 991/MK-8722 (∼1.5−2-fold). However, the results from this assay do not reflect cellular activity, as the *in vitro* kinase assay following immunoprecipitation accounts for covalently-regulated activity (e.g. phosphorylation), but not allosterically-regulated (i.e. by AMP/ZMP, 991/MK-8722) activity. Judging from phosphorylation levels of ACC and TBC1D1, AICAR and 991/MK-8722 comparably increased cellular AMPK activity in skeletal muscle. However, notably, compound-induced phosphorylation of ACC and TBC1D1 *ex vivo* was only reduced in EDL when treated with AICAR, but not with 991/MK-8722, in γ3 KO compared to WT. This raises the possibility that AICAR preferentially activates γ3- over γ1-containing complex(es). Concordantly, AMP appears to have stronger binding affinity to nucleotide binding site 3 (in the CBS domain) of γ3 (∼40 μM) than γ1 (∼300−600 μM) *in vitro* (using bacterial AMPK-complex preparations) [53]. Conversely, another *in vitro* study reported that while AMP potently (allosterically) activated α2β2γ1 (∼3-fold), it barely activated α2β2γ3 (<15%) complex [54]. Thus, how these *in vitro* results can be interpreted and translated into cellular context remain unclear. The γ-isoforms all contain a highly conserved C-terminal region harboring the four CBS domains. Conversely, the γ2 and γ3 isoforms contain long N-terminal extensions that are not present in the γ1 isoform. These N-terminal extensions display no apparent sequence conservation between isoforms. To date, there are no crystal structures available for γ2- or γ3-containing AMPK trimeric complexes and it is unknown whether the N-terminal extensions of γ2 or γ3 play any functional role. A recent study using cell-based assays demonstrated that α2β2γ1 and α2β2γ3 complexes were similarly activated in response to 991 treatment, whereas α2β2γ2 complexes exhibited a greater activation (compared to α2β2γ1/α2β2γ3 complexes) [55]. The authors proposed that the effect is mediated by the N-terminal region of γ2 and is due to enhanced protection of AMPKα Thr172 from dephosphorylation. Whether N-terminal extension of γ3 has any specific role to play in muscle cells/tissue and in AMP/ZMP-mediated regulation of AMPK and glucose uptake in skeletal muscle is unknown. Even though γ3 deficiency was associated with reduced AICAR-stimulated glucose uptake in EDL muscle *ex vivo*, we provide the first evidence that the AICAR-induced blood glucose lowering effect *in vivo* was robustly reduced in γ3 KO compared to WT mice, which was quite similar to AMPKα2 KO and α2 kinase-dead (KD) expressing transgenic mice [28,30]. Indeed, α2 KO and KD mice still showed decreases in blood glucose in response to an acute injection of AICAR, which is most likely due to the inhibitory effect of AICAR on hepatic glucose production through ZMP-dependent inhibition of fructose 1,6-bisphosphatase 1 [13,56]. MK-8722 has been shown to cause blood glucose-lowering effect through the stimulation of glucose uptake in both glycolytic (GAS) and oxidative (soleus) muscle *in vivo* [24]. In contrast to AICAR, but consistent with *ex vivo* data, we provided evidence that MK-8722-induced skeletal muscle glucose uptake and blood glucose-lowering effects were comparable between γ3 KO and WT mice. This compellingly demonstrates that γ3 is dispensable (in other words γ1 and its containing α2β2γ1 complex is sufficient) in stimulating glucose uptake in skeletal muscle in response to pan-AMPK ADaM site-binding activators. To further test this proposition, it would be of interest to generate and study a skeletal muscle-specific and inducible AMPKγ1 KO mouse model.

Evidence suggests that AMPK plays a vital role in regulating the development of BAT, maintenance of BAT mitochondrial function, and browning of WAT [35]. We provided genetic evidence that mice lacking functional AMPK specifically in adipocytes, through an inducible deletion of β1 and β2, were intolerant to cold and resistant to β-adrenergic stimulation of brown and beige adipose tissues [36]. Similar findings were also observed in AMPK α1/α2 KO mice [57]. Detailed protein expression profiles of AMPK subunit isoforms in BAT in comparison to other tissues have not been performed, and to our knowledge, the presence of γ3 protein in BAT has not been demonstrated. RNA sequencing results identified γ3 at intermediate amounts (Reads Per Kilobase of transcript per Million mapped reads, >40) in mouse brown preadipocytes [37]. Strikingly, RNAi-mediated knockdown of either γ1 or γ3 (but not γ2) in brown adipocyte precursors was sufficient to profoundly reduce (>80%) UCP1 protein expression. Using γ3-specific antibodies we developed, we have demonstrated that γ3 protein/activity is present and in complex mainly with α2 and β2 in mouse BAT. Even though we showed that γ3 is dispensable for β-adrenergic-induced thermogenesis and remodeling of BAT and iWAT, future studies are warranted to determine whether the specific activation of the γ3-containing complexes (when such drugs are available) induces adipose browning and subsequent amelioration of insulin resistance and fatty liver disease.

5. CONCLUSIONS

We demonstrated that a genetic loss of γ3 resulted in a selective loss of AICAR-stimulated glucose-lowering *in vivo* and glucose uptake specifically in glycolytic skeletal muscles *ex vivo*. We also showed that γ3 is dispensable for thermogenesis and the browning of WAT. The potent pan-AMPK activators targeting the ADaM site are effective in reversing hyperglycemia in rodents and non-human primates, and this is due to activation of AMPK in skeletal muscle, not in the liver [23,24].

This might make them valuable adjuncts to metformin, which acts primarily on the liver [13,58,59]. However, there are remaining important safety issues that need to be carefully considered and examined, such as the potential for AMPK activation to promote cardiac hypertrophy or the survival of cancer cells (e.g. under hypoxic conditions). To avoid these potential liabilities, the development of AMPK activators that can be targeted to specific tissues (for example, the liver, muscle, and adipose) by taking advantage of isoform-specific selectivity may be beneficial. We and others have shown that selective targeting of specific AMPK isoforms (e.g. α1, β1) by small molecules is possible [9,60,61]. The current study provides key insights that ADaM site binding compounds will not be selective for γ3-containing complex and skeletal muscle-selective AMP-mimetics may provide beneficial effects on glycemia in people with type 2 diabetes. Nevertheless, when a γ3-complex selective activator is available in the future, ascertaining whether it sufficiently promotes skeletal muscle glucose uptake without causing cardiac hypertrophy and glycogen accumulation will be of major interest.

AUTHOR CONTRIBUTIONS

Conceptualization: K.S. Experimental design: P.Rh., E.M.D., P.R., D.A., N.B., J.S., M.D.S., A.J.O., M.F.K., G.R.S., K.S. Experimental execution: P.Rh., E.M.D., P.R., D.A., N.B., J.S., M.D.S., A.J.O., J.M.Y., A.M.E., J.L.S.G., Q.O., J.M.Y., M.F.K., M.M. Supervision: J.S., N.J., J.S.O., J.T.T., P.M., J.W.S., M.J.S, P.D., S.C., G.R.S., K.S. Writing — Original draft preparation: K.S., P.Rh. Writing — Reviewing and Editing: All authors.

GRANTS

This study was supported by the Novo Nordisk Foundation (NNF20OC0063515) to K.S. E.M.D. is a Vanier Canada Graduate Scholar. G.R.S. is supported by a Diabetes Canada Investigator Award (DI-5-17-5302-GS), a Canadian Institutes of Health Research Foundation Grant (201709FDN-CEBA-116200), a Tier 1 Canada Research Chair and a J. Bruce Duncan Endowed Chair in Metabolic Diseases. This study was also supported by the Ministry of Science and Technology of China (Grant No. 2018YFA0801102 to S.C.). The P.M. lab is funded by the Association Française contre les Myopathies (AFM n°21711), and by the Agence Nationale pour la Recherche (Myolinc, ANR R17062KK). J.W.S. and J.S.O. were supported by National Health and Medical Research Council (NHMRC) project grants (GNT1138102 and GNT1145265, respectively). This project was supported in part by the Victorian Government's Operational Infrastructure Support Program. A.J.O. is supported by a PhD scholarship funded by the Australian Catholic University. M.F.K. has received funding from Danish Diabetes Academy and Novo Nordisk Foundation. Novo Nordisk Foundation Center for Basic Metabolic Research is an independent Research Center based at the University of Copenhagen, Denmark, and partially funded by an unconditional donation from the Novo Nordisk Foundation (Grant number NNF18CC0034900).

ACKNOWLEDGMENTS

We thank Carles Canto, Magali Joffraud, Guillaume Jacot, Maria Deak, Caterina Collodet, Alix Zollinger, Sylviane Metairon, and Stefan Christen (all affiliated with Nestlé Research) for their technical assistance and input for experimental design, assays, and data analysis/interpretation. We also thank Juleen Zierath for her critical review of the manuscript.

CONFLICT OF INTEREST

P.Rh., P.D., J.S., M.J.S., J.L.S.G., and M.M. are current and N.B. and K.S. were former employees of Nestlé Research (Switzerland).

APPENDIX A. SUPPLEMENTARY DATA

Supplementary data to this article can be found online at https://doi.org/10.1016/j.molmet.2021.101228.

REFERENCES

[1] Hardie, D.G., 2011. AMP-activated protein kinase: an energy sensor that regulates all aspects of cell function. Genes & Development 25(18):1895—1908.

[2] Herzig, S., Shaw, R.J., 2018. AMPK: guardian of metabolism and mitochondrial homeostasis. Nature Reviews Molecular Cell Biology 19(2):121—135.

[3] Hawley, S.A., Davison, M., Woods, A., Davies, S.P., Beri, R.K., Carling, D., et al., 1996. Characterization of the AMP-activated protein kinase kinase from rat liver and identification of threonine 172 as the major site at which it phosphorylates AMP-activated protein kinase. Journal of Biological Chemistry 271(44):27879—27887.

[4] Sakamoto, K., McCarthy, A., Smith, D., Green, K.A., Grahame Hardie, D., Ashworth, A., et al., 2005. Deficiency of LKB1 in skeletal muscle prevents AMPK activation and glucose uptake during contraction. The EMBO Journal 24(10):1810—1820.

[5] Shaw, R.J., Lamia, K.A., Vasquez, D., Koo, S.H., Bardeesy, N., Depinho, R.A., et al., 2005. The kinase LKB1 mediates glucose homeostasis in liver and therapeutic effects of metformin. Science 310(5754):1642—1646.

[6] Gowans, G.J., Hawley, S.A., Ross, F.A., Hardie, D.G., 2013. AMP is a true physiological regulator of AMP-activated protein kinase by both allosteric activation and enhancing net phosphorylation. Cell Metabolism 18(4):556—566.

[7] Xiao, B., Sanders, M.J., Underwood, E., Heath, R., Mayer, F.V., Carmena, D., et al., 2011. Structure of mammalian AMPK and its regulation by ADP. Nature 472(7342):230—233.

[8] Oakhill, J.S., Steel, R., Chen, Z.P., Scott, J.W., Ling, N., Tam, S., et al., 2011. AMPK is a direct adenylate charge-regulated protein kinase. Science 332(6036):1433—1435.

[9] Steinberg, G.R., Carling, D., 2019. AMP-activated protein kinase: the current landscape for drug development. Nature Reviews Drug Discovery 18(7):527—551.

[10] Buhl, E.S., Jessen, N., Pold, R., Ledet, T., Flyvbjerg, A., Pedersen, S.B., et al., 2002. Long-term AICAR administration reduces metabolic disturbances and lowers blood pressure in rats displaying features of the insulin resistance syndrome. Diabetes 51(7):2199—2206.

[11] Guigas, B., Sakamoto, K., Taleux, N., Reyna, S.M., Musi, N., Viollet, B., et al., 2009. Beyond AICA riboside: in search of new specific AMP-activated protein kinase activators. IUBMB Life 61(1):18—26.

[12] Foretz, M., Hebrard, S., Leclerc, J., Zarrinpashneh, E., Soty, M., Mithieux, G., et al., 2010. Metformin inhibits hepatic gluconeogenesis in mice independently of the LKB1/AMPK pathway via a decrease in hepatic energy state. Journal of Clinical Investigation 120(7):2355—2369.

[13] Hunter, R.W., Hughey, C.C., Lantier, L., Sundelin, E.I., Peggie, M., Zeqiraj, E., et al., 2018. Metformin reduces liver glucose production by inhibition of fructose-1-6-bisphosphatase. Nature Medicine 24(9):1395—1406.

[14] Collodet, C., Foretz, M., Deak, M., Bultot, L., Metairon, S., Viollet, B., et al., 2019. AMPK promotes induction of the tumor suppressor FLCN through activation of TFEB independently of mTOR. The FASEB Journal 33(11):12374–12391.

[15] Cool, B., Zinker, B., Chiou, W., Kifle, L., Cao, N., Perham, M., et al., 2006. Identification and characterization of a small molecule AMPK activator that treats key components of type 2 diabetes and the metabolic syndrome. Cell Metabolism 3(6):403–416.

[16] Goransson, O., McBride, A., Hawley, S.A., Ross, F.A., Shpiro, N., Foretz, M., et al., 2007. Mechanism of action of A-769662, a valuable tool for activation of AMP-activated protein kinase. Journal of Biological Chemistry 282(45): 32549–32560.

[17] Scott, J.W., van Denderen, B.J., Jorgensen, S.B., Honeyman, J.E., Steinberg, G.R., Oakhill, J.S., et al., 2008. Thienopyridone drugs are selective activators of AMP-activated protein kinase beta1-containing complexes. Chemistry & Biology 15(11):1220–1230.

[18] Sanders, M.J., Ali, Z.S., Hegarty, B.D., Heath, R., Snowden, M.A., Carling, D., 2007. Defining the mechanism of activation of AMP-activated protein kinase by the small molecule A-769662, a member of the thienopyridone family. Journal of Biological Chemistry 282(45):32539–32548.

[19] Xiao, B., Sanders, M.J., Carmena, D., Bright, N.J., Haire, L.F., Underwood, E., et al., 2013. Structural basis of AMPK regulation by small molecule activators. Nature Communications 4:3017.

[20] Calabrese, M.F., Rajamohan, F., Harris, M.S., Caspers, N.L., Magyar, R., Withka, J.M., et al., 2014. Structural basis for AMPK activation: natural and synthetic ligands regulate kinase activity from opposite poles by different molecular mechanisms. Structure 22(8):1161–1172.

[21] Treebak, J.T., Birk, J.B., Hansen, B.F., Olsen, G.S., Wojtaszewski, J.F., 2009. A-769662 activates AMPK beta1-containing complexes but induces glucose uptake through a PI3-kinase-dependent pathway in mouse skeletal muscle. American Journal of Physiology – Cell Physiology 297(4):C1041–C1052.

[22] Bultot, L., Jensen, T.E., Lai, Y.C., Madsen, A.L., Collodet, C., Kviklyte, S., et al., 2016. Benzimidazole derivative small-molecule 991 enhances AMPK activity and glucose uptake induced by AICAR or contraction in skeletal muscle. American Journal of Physiology. Endocrinology and Metabolism 311(4):E706–E719.

[23] Cokorinos, E.C., Delmore, J., Reyes, A.R., Albuquerque, B., Kjobsted, R., Jorgensen, N.O., et al., 2017. Activation of skeletal muscle AMPK promotes glucose disposal and glucose lowering in non-human primates and mice. Cell Metabolism 25(5), 1147–1159, e1110.

[24] Myers, R.W., Guan, H.P., Ehrhart, J., Petrov, A., Prahalada, S., Tozzo, E., et al., 2017. Systemic pan-AMPK activator MK-8722 improves glucose homeostasis but induces cardiac hypertrophy. Science 357(6350):507–511.

[25] Barnes, B.R., Marklund, S., Steiler, T.L., Walter, M., Hjalm, G., Amarger, V., et al., 2004. The 5′-AMP-activated protein kinase gamma3 isoform has a key role in carbohydrate and lipid metabolism in glycolytic skeletal muscle. Journal of Biological Chemistry 279(37):38441–38447.

[26] Mahlapuu, M., Johansson, C., Lindgren, K., Hjalm, G., Barnes, B.R., Krook, A., et al., 2004. Expression profiling of the gamma-subunit isoforms of AMP-activated protein kinase suggests a major role for gamma3 in white skeletal muscle. American Journal of Physiology. Endocrinology and Metabolism 286(2):E194–E200.

[27] Yu, H., Fujii, N., Hirshman, M.F., Pomerleau, J.M., Goodyear, L.J., 2004. Cloning and characterization of mouse 5′-AMP-activated protein kinase gamma3 subunit. American Journal of Physiology – Cell Physiology 286(2): C283–C292.

[28] Mu, J., Brozinick Jr., J.T., Valladares, O., Bucan, M., Birnbaum, M.J., 2001. A role for AMP-activated protein kinase in contraction- and hypoxia-regulated glucose transport in skeletal muscle. Molecular Cell 7(5):1085–1094.

[29] Fujii, N., Hirshman, M.F., Kane, E.M., Ho, R.C., Peter, L.E., Seifert, M.M., et al., 2005. AMP-activated protein kinase alpha2 activity is not essential for contraction- and hyperosmolarity-induced glucose transport in skeletal muscle. Journal of Biological Chemistry 280(47):39033–39041.

[30] Jorgensen, S.B., Viollet, B., Andreelli, F., Frosig, C., Birk, J.B., Schjerling, P., et al., 2004. Knockout of the alpha2 but not alpha1 5′-AMP-activated protein kinase isoform abolishes 5-aminoimidazole-4-carboxamide-1-beta-4-ribofuranosidebut not contraction-induced glucose uptake in skeletal muscle. Journal of Biological Chemistry 279(2):1070–1079.

[31] Steinberg, G.R., O'Neill, H.M., Dzamko, N.L., Galic, S., Naim, T., Koopman, R., et al., 2010. Whole body deletion of AMP-activated protein kinase {beta}2 reduces muscle AMPK activity and exercise capacity. Journal of Biological Chemistry 285(48):37198–37209.

[32] Dasgupta, B., Ju, J.S., Sasaki, Y., Liu, X., Jung, S.R., Higashida, K., et al., 2012. The AMPK beta2 subunit is required for energy homeostasis during metabolic stress. Molecular and Cellular Biology 32(14):2837–2848.

[33] Hardie, D.G., Sakamoto, K., 2006. AMPK: a key sensor of fuel and energy status in skeletal muscle. Physiology 21:48–60.

[34] Kjobsted, R., Hingst, J.R., Fentz, J., Foretz, M., Sanz, M.N., Pehmoller, C., et al., 2018. AMPK in skeletal muscle function and metabolism. The FASEB Journal 32(4):1741–1777.

[35] Desjardins, E.M., Steinberg, G.R., 2018. Emerging role of AMPK in Brown and beige adipose tissue (BAT): implications for obesity, insulin resistance, and type 2 diabetes. Current Diabetes Reports 18(10):80.

[36] Mottillo, E.P., Desjardins, E.M., Crane, J.D., Smith, B.K., Green, A.E., Ducommun, S., et al., 2016. Lack of adipocyte AMPK exacerbates insulin resistance and hepatic steatosis through brown and beige adipose tissue function. Cell Metabolism 24(1):118–129.

[37] Perdikari, A., Kulenkampff, E., Rudigier, C., Neubauer, H., Luippold, G., Redemann, N., et al., 2017. A high-throughput, image-based screen to identify kinases involved in brown adipocyte development. Science Signaling 10(466).

[38] Nakada, D., Saunders, T.L., Morrison, S.J., 2010. Lkb1 regulates cell cycle and energy metabolism in haematopoietic stem cells. Nature 468(7324):653–658.

[39] Dos Santos, M., Backer, S., Saintpierre, B., Izac, B., Andrieu, M., Letourneur, F., et al., 2020. Single-nucleus RNA-seq and FISH identify coordinated transcriptional activity in mammalian myofibers. Nature Communications 11(1):5102.

[40] Shi, H., Munk, A., Nielsen, T.S., Daughtry, M.R., Larsson, L., Li, S., et al., 2018. Skeletal muscle O-GlcNAc transferase is important for muscle energy homeostasis and whole-body insulin sensitivity. Molecular Metabolism 11:160–177.

[41] Chen, Q., Xie, B., Zhu, S., Rong, P., Sheng, Y., Ducommun, S., et al., 2017. A Tbc1d1 (Ser231Ala)-knockin mutation partially impairs AICAR- but not exercise-induced muscle glucose uptake in mice. Diabetologia 60(2):336–345.

[42] Dite, T.A., Langendorf, C.G., Hoque, A., Galic, S., Rebello, R.J., Ovens, A.J., et al., 2018. AMP-activated protein kinase selectively inhibited by the type II inhibitor SBI-0206965. Journal of Biological Chemistry 293(23):8874–8885.

[43] Scott, J.W., Galic, S., Graham, K.L., Foitzik, R., Ling, N.X., Dite, T.A., et al., 2015. Inhibition of AMP-activated protein kinase at the allosteric drug-binding site promotes islet insulin release. Chemistry & Biology 22(6):705–711.

[44] Crane, J.D., Mottillo, E.P., Farncombe, T.H., Morrison, K.M., Steinberg, G.R., 2014. A standardized infrared imaging technique that specifically detects UCP1-mediated thermogenesis in vivo. Molecular Metabolism 3(4):490–494.

[45] O'Neill, H.M., Maarbjerg, S.J., Crane, J.D., Jeppesen, J., Jorgensen, S.B., Schertzer, J.D., et al., 2011. AMP-activated protein kinase (AMPK) beta1beta2 muscle null mice reveal an essential role for AMPK in maintaining mitochondrial content and glucose uptake during exercise. Proceedings of the National Academy of Sciences of the United States of America 108(38): 16092–16097.

[46] Fentz, J., Kjobsted, R., Birk, J.B., Jordy, A.B., Jeppesen, J., Thorsen, K., et al., 2015. AMPKalpha is critical for enhancing skeletal muscle fatty acid utilization during in vivo exercise in mice. The FASEB Journal 29(5):1725–1738.

[47] Lantier, L., Fentz, J., Mounier, R., Leclerc, J., Treebak, J.T., Pehmoller, C., et al., 2014. AMPK controls exercise endurance, mitochondrial oxidative capacity, and skeletal muscle integrity. The FASEB Journal 28(7):3211—3224.

[48] Zong, H., Ren, J.M., Young, L.H., Pypaert, M., Mu, J., Birnbaum, M.J., et al., 2002. AMP kinase is required for mitochondrial biogenesis in skeletal muscle in response to chronic energy deprivation. Proceedings of the National Academy of Sciences of the United States of America 99(25):15983—15987.

[49] Garcia-Roves, P.M., Osler, M.E., Holmstrom, M.H., Zierath, J.R., 2008. Gain-of-function R225Q mutation in AMP-activated protein kinase gamma3 subunit increases mitochondrial biogenesis in glycolytic skeletal muscle. Journal of Biological Chemistry 283(51):35724—35734.

[50] Lai, Y.C., Kviklyte, S., Vertommen, D., Lantier, L., Foretz, M., Viollet, B., et al., 2014. A small-molecule benzimidazole derivative that potently activates AMPK to increase glucose transport in skeletal muscle: comparison with effects of contraction and other AMPK activators. Biochemical Journal 460(3):363—375.

[51] Foretz, M., Hebrard, S., Guihard, S., Leclerc, J., Do Cruzeiro, M., Hamard, G., et al., 2011. The AMPKgamma1 subunit plays an essential role in erythrocyte membrane elasticity, and its genetic inactivation induces splenomegaly and anemia. The FASEB Journal 25(1):337—347.

[52] Treebak, J.T., Birk, J.B., Rose, A.J., Kiens, B., Richter, E.A., Wojtaszewski, J.F., 2007. AS160 phosphorylation is associated with activation of alpha2beta2gamma1- but not alpha2beta2gamma3-AMPK trimeric complex in skeletal muscle during exercise in humans. American Journal of Physiology. Endocrinology and Metabolism 292(3):E715—E722.

[53] Rajamohan, F., Reyes, A.R., Frisbie, R.K., Hoth, L.R., Sahasrabudhe, P., Magyar, R., et al., 2016. Probing the enzyme kinetics, allosteric modulation and activation of alpha1- and alpha2-subunit-containing AMP-activated protein kinase (AMPK) heterotrimeric complexes by pharmacological and physiological activators. Biochemical Journal 473(5):581—592.

[54] Ross, F.A., Jensen, T.E., Hardie, D.G., 2016. Differential regulation by AMP and ADP of AMPK complexes containing different gamma subunit isoforms. Biochemical Journal 473(2):189—199.

[55] Willows, R., Navaratnam, N., Lima, A., Read, J., Carling, D., 2017. Effect of different gamma-subunit isoforms on the regulation of AMPK. Biochemical Journal 474(10):1741—1754.

[56] Vincent, M.F., Erion, M.D., Gruber, H.E., Van den Berghe, G., 1996. Hypoglycaemic effect of AICAriboside in mice. Diabetologia 39(10):1148—1155.

[57] Wu, L., Zhang, L., Li, B., Jiang, H., Duan, Y., Xie, Z., et al., 2018. AMP-activated protein kinase (AMPK) regulates energy metabolism through modulating thermogenesis in adipose tissue. Frontiers in Physiology 9:122.

[58] Fullerton, M.D., Galic, S., Marcinko, K., Sikkema, S., Pulinilkunnil, T., Chen, Z.P., et al., 2013. Single phosphorylation sites in Acc1 and Acc2 regulate lipid homeostasis and the insulin-sensitizing effects of metformin. Nature Medicine 19(12):1649—1654.

[59] Rena, G., Pearson, E.R., Sakamoto, K., 2013. Molecular mechanism of action of metformin: old or new insights? Diabetologia 56(9):1898—1906.

[60] Hunter, R.W., Foretz, M., Bultot, L., Fullerton, M.D., Deak, M., Ross, F.A., et al., 2014. Mechanism of action of compound-13: an alpha1-selective small molecule activator of AMPK. Chemistry & Biology 21(7):866—879.

[61] Langendorf, C.G., Ngoei, K.R.W., Scott, J.W., Ling, N.X.Y., Issa, S.M.A., Gorman, M.A., et al., 2016. Structural basis of allosteric and synergistic activation of AMPK by furan-2-phosphonic derivative C2 binding. Nature Communications 7:10912.

